J. Fluid Mech. (1995), *vol.* 297, *pp.* 373–401

Time-dependent transport by convection and diffusion with exchange between two phases

By C. G. PHILLIPS[1,2], S. R. KAYE[1] AND C. D. ROBINSON[1]

[1]Physiological Flow Studies Group, Centre for Biological and Medical Systems, Imperial College of Science, Technology and Medicine, Prince Consort Road, London SW7 2BY, UK

[2]Department of Mathematics, Imperial College of Science, Technology and Medicine, Prince Consort Road, London SW7 2BY, UK

(Received 26 July 1994 and in revised form 4 April 1995)

We consider the transport of a tracer substance through a system consisting of a tube containing flowing fluid surrounded by a wall layer in which the tracer is soluble. The fluid moves with either a Poiseuille or a uniform flow profile, and the outer boundary of the wall layer is either impermeable to tracer or absorbs it perfectly. The development of dispersive transport following the injection of tracer is described in terms of three time-dependent effective transport coefficients, viz. the fraction of tracer remaining in the system, the apparent convection velocity and the dispersion coefficient; the last two are defined in terms of the rates of change of the mean and variance of the axial tracer distribution. We assume that the timescale for tracer diffusion across the wall layer is much larger than that for diffusion across the flowing phase, and derive an asymptotic approximation corresponding to each timescale. Numerical results are given to illustrate sensitivity to the physical parameters of the system. It is shown that if the coefficients are based on tracer concentration in the fluid phase alone, as in previous work, paradoxical behaviour, such as negative apparent convection velocities, can result; we therefore base our results on averages of concentration over both phases. On the shorter timescale (the same timescale over which Taylor dispersion develops) at leading order it is found that the influence of the wall layer can be characterized by a single dimensionless parameter, and that conditions at the outer boundary have no effect. In many cases transport is also rather insensitive to the form of the flow profile. On the longer timescale, at leading order the influence of the wall layer is characterized by another dimensionless parameter, and unless uptake is very small diffusion within the layer is the rate-determining process; consequently transport is independent of the form of the flow profile. A further important conclusion is that the usual effective convection and dispersion coefficients, based on spatial moments, are of little use in predicting the time-varying concentration at a fixed position, because the spatial concentration profile becomes Gaussian only over the longer timescale.

1. Introduction

In this paper we consider theoretically the time-dependent transport of a tracer substance, by convection and diffusion, in a system consisting of a tube containing a flowing fluid surrounded by a stationary annular wall layer in which the tracer is soluble but diffuses much more slowly than in the fluid. The outer boundary of

the wall layer is considered either to be impermeable to the tracer, or to absorb it perfectly. In addition to convection arising directly from the movement of the fluid, the tracer experiences dispersion, i.e. an enhanced effective diffusivity in the direction of flow, both as a result of the non-uniformity of the flow field, and due to the exchange of the substance with the wall layer.

In its most general form the problem of transport through a medium composed of both a flowing fluid and a stationary component in which diffusion is restricted is relevant to a very wide range of transport processes. For example, the fluid can be either gas (when the stationary layer could be a liquid lining) or liquid (when it could be a gel layer), and the mathematical formulation is applicable not only to mass transport, but also to heat (when the flowing phase could be a liquid, and the stationary phase a solid of relatively small thermal diffusivity). Such systems occur commonly in chemical engineering, where tubular geometries are used in gas and liquid chromatography and other separation processes. In biology, the same mechanisms are responsible for the transport of soluble gases in the airways of the lung, which will be discussed further below, and of solutes in blood vessels. An accurate model of transport in blood vessels is desirable both for the understanding of normal physiological function (cf. the Krogh 'tissue cylinder' model for transfer from capillary vessels) and for the interpretation of experimental methods (e.g. the thermal–dye dilution technique).

The basic process of solute dispersion as a result of diffusion in, and convection by, Poiseuille flow in a tube with impermeable walls was originally studied by Taylor (1953, 1954) and Aris (1956). After a timescale much larger than that required for a tracer molecule to diffuse across the tube, the solute distribution was found to move along the tube with the same average speed as the fluid, and to spread axially with an apparent diffusion coefficient greater than its true (molecular) value. This coefficient was expressed as the sum of two terms, the first reflecting the effect of axial convection combined with radial diffusion (because each solute molecule diffuses through regions of fluid moving with different speeds) and the second resulting directly from axial diffusion. Aris later (1959) considered dispersion in a system with annular geometry, containing both a flowing phase and a stationary phase in which the tracer is soluble. The apparent axial diffusion coefficient at long times contains convective and diffusive components, consisting of weighted averages of contributions from the two phases, together with a third term resulting from the presence in Aris's model of a resistive barrier to exchange between the phases. Both Taylor's and Aris' solutions are for the steady value of the dispersion coefficient at long times, which we shall refer to as 'fully developed' dispersion.

The time-development of dispersion has most commonly been studied by calculating the evolution with time of the axial moments of the tracer concentration following its injection into the flow. Thus, Gill & Sankarasubramanian (1970) considered the development of Taylor–Aris dispersion, calculating a time-dependent 'dispersion coefficient', equal to half the rate of change of the variance of the axial tracer concentration profile. For application in a model of the bronchial tree, Davidson & Schroter (1983) calculated the rates of change of both the mean and variance, based on averages of concentration in the fluid phase, in a two-phase system in which the fluid moves with Poiseuille flow, and there is a stationary wall layer surrounded by an impermeable outer boundary. More recently, Shankar & Lenhoff (1991) have calculated tracer concentration profiles as a function of space and time for the same system (but neglecting axial diffusion), for cases where the timescales for diffusion across the fluid phase and the wall layer are comparable.

In many applications, including biological systems such as the bronchial airways or the vascular tree, transport takes place through a network of branching tubes, each of which may be only a few times longer than it is wide. As a result, in addition to dispersion itself not being fully developed, the flow field within each tube is developing and cannot be described by Poiseuille's solution. Another complication in biological applications is the possible removal of tracer from the system, for example by the capillary blood vessels surrounding arteries and airways. For fully developed dispersion, some of these effects have been addressed theoretically. For example, Aris' (1956) formulation for dispersion in a single flowing phase dealt, in principle, with an arbitrary (but axially invariant) velocity profile. The case where tracer is (irreversibly) absorbed at the outer boundary of a single flowing phase, at a rate proportional to the local concentration, has been studied by several workers, either for fully developed dispersion or at long times (e.g. Sankarasubramanian & Gill 1973; Lungu & Moffatt 1982; Smith 1983). A more general boundary condition incorporating history-dependence was used by Purnama (1988), who calculated the fully developed dispersion coefficient (this formalism could be used to describe the effects of the wall layer considered in the present work). Despite these treatments, for transient dispersion as opposed to the fully developed process, the effects of tracer absorption and desorption by a wall layer, and the sensitivity to the flow profile, are poorly understood.

The objective of this paper is to investigate the dominant mechanisms and timescales in the transient transport of a tracer by convection, diffusion and exchange with a stationary absorbing medium, and to evaluate its sensitivity to the physical parameters, the form of the flow field and the boundary conditions imposed. In order to do so we consider a model system similar to that of Davidson & Schroter (1983), in which a tube containing moving fluid is surrounded by an annular, stationary wall layer. Tracer is initially distributed within the fluid phase, with an arbitrary axial concentration distribution (provided the axial moments defined below are finite) and with the concentration assumed uniform within each cross-section. Subsequently it diffuses and is convected in the fluid phase, and can be absorbed into (and desorbed from) the wall layer, where transport is due to diffusion alone. We consider two possible conditions at the outer boundary of the wall layer: a boundary impermeable to tracer (as assumed by Davidson & Schroter) and one which absorbs tracer perfectly. We also compare the results obtained assuming Poiseuille flow to those obtained for a hypothetical situation in which there is a uniform axial fluid velocity.

In §2 we give the mathematical formulation of the problem, and define three effective transport coefficients, which vary as functions of time following the introduction of tracer into the flow, viz. the fraction of tracer remaining in the system, an apparent convection coefficient, and a dispersion coefficient. These coefficients are defined either with reference to the concentration in the fluid phase alone (as Davidson & Schroter) or by including the contribution of the wall layer. The full model problem is governed by four dimensionless parameters (defined by (2.6)). Our solutions are based on the range of parameter values appropriate to the transport of highly soluble gases in the human bronchial tree (Davidson & Schroter). For these values, it is possible to make simplifying assumptions, which allow perturbation methods to be used to derive analytic approximations to the solution (in §3), rather than solving the full problem numerically. The primary assumption is that the tracer takes much longer to diffuse across the wall layer than across the fluid-filled tube, which means that the development of dispersion takes place over two widely separated timescales, for each of which a simplified approximate solution exists. Furthermore, we assume

that the wall layer is sufficiently thin that its curvature can be neglected, and that uptake of tracer by the wall layer is not so small that transport in the fluid phase is rate-determining (see §3.3). As well as simplifying the mathematical problem, this approach has the virtue of revealing clearly the dominant physical mechanisms that operate, and the dimensionless parameters that govern them. Numerical results are given in §4, and in §5 the results are discussed, and the relationship with previous studies and implications for future work are considered.

2. The general problem

2.1. *Formulation and definition of transport coefficients*

Denote the tracer concentration by C and time by T, and use (dimensional) cylindrical polar coordinates with Z representing axial, and R radial, distance. Assuming that the initial concentration and the velocity profile are axisymmetric, the governing equations in the fluid and the wall layer respectively are

$$\frac{\partial C}{\partial T} + V(R)\frac{\partial C}{\partial Z} = D\left\{R^{-1}\frac{\partial}{\partial R}\left(R\frac{\partial C}{\partial R}\right) + \frac{\partial^2 C}{\partial Z^2}\right\} \qquad \text{for } 0 \leqslant R < a, \tag{2.1a}$$

$$\frac{\partial C}{\partial T} = D_w\left\{R^{-1}\frac{\partial}{\partial R}\left(R\frac{\partial C}{\partial R}\right) + \frac{\partial^2 C}{\partial Z^2}\right\} \qquad \text{for } a < R < a+h, \tag{2.1b}$$

in which $V(R)$ is the axial fluid velocity, a is the radius of the tube, h the wall layer thickness, and the diffusion coefficient of the tracer is denoted by D for the fluid and D_w for the wall layer. The boundary conditions at the interface between the two phases are

$$C|_{R=a^+} = \beta C|_{R=a^-}, \qquad D_w\frac{\partial C}{\partial R}\bigg|_{R=a^+} = D\frac{\partial C}{\partial R}\bigg|_{R=a^-}, \tag{2.2}$$

in which β is the ratio of the tracer concentration in the wall phase to that in the fluid phase at equilibrium. Note that we assume there is no resistance to the exchange of tracer at the interface, so that the concentrations in the fluid and wall phase are locally in equilibrium. The existence of a resistive barrier at the interface would further complicate the results (cf. Aris 1959).

The problem of heat transport is mathematically equivalent to that of mass transport, and is obtained if C represents temperature, D the thermal diffusivity and β is set equal to unity, since the temperature is continuous across the interface with the wall layer.

The solution is required to be regular on the tube axis ($R = 0$), and an additional boundary condition is required at the outer boundary of the wall layer ($R = a + h$). In the present work we consider two extreme cases. The first,

$$\frac{\partial C}{\partial R}\bigg|_{R=a+h} = 0, \tag{2.3}$$

corresponds to an impermeable boundary outside the wall layer (this is the boundary condition used by Davidson & Schroter 1983); the other,

$$C|_{R=a+h} = 0, \tag{2.4}$$

represents a perfectly absorbing boundary outside the wall layer. Since the problem is linear, the effective transport coefficients defined by (2.11)–(2.13) below do not depend on the initial concentration distribution in the fluid phase, provided it is independent

of R. It is therefore sufficient to solve the problem for the initial condition

$$C|_{T=0} = M\delta(Z)\theta(a-R)/\pi a^2, \tag{2.5}$$

which represents tracer uniformly distributed over the cross-section of the fluid phase at $Z = 0$; M is the total mass of tracer present initially, δ is the Dirac delta function and θ is the Heaviside function.

We define four dimensionless parameters

$$\lambda = D_w/D, \qquad \kappa = (D_w/D)^{1/2}\beta, \qquad P = V_0 a/D, \qquad \epsilon = h/a, \tag{2.6}$$

in which V_0 is the average axial fluid velocity; λ is the ratio of the diffusion coefficient in the wall layer to that in the fluid, P is the Péclet number, which expresses the strength of convection relative to that of diffusion in the fluid, ϵ reflects the importance of the curvature of the wall layer, and κ, which we shall refer to as the dimensionless absorption parameter, incorporates both the ratio of tracer concentrations across the interface and the ratio of the diffusion coefficients in the wall layer and fluid. The governing equations and boundary conditions are non-dimensionalized by defining the variables

$$c = \pi P a^3 C/M, \qquad r = R/a, \qquad z = Z/Pa, \qquad t = DT/a^2, \tag{2.7}$$

in which time is non-dimensionalized with respect to the timescale for diffusion across the interior of the tube. Note that the lengthscales used to non-dimensionalize the radial and axial variables are different. In terms of these variables the governing equations and boundary conditions become

$$\frac{\partial c}{\partial t} + v(r)\frac{\partial c}{\partial z} = r^{-1}\frac{\partial}{\partial r}\left(r\frac{\partial c}{\partial r}\right) + P^{-2}\frac{\partial^2 c}{\partial z^2} \qquad \text{for } 0 \leqslant r < 1, \tag{2.8a}$$

$$\frac{\partial c}{\partial t} = \lambda\left\{r^{-1}\frac{\partial}{\partial r}\left(r\frac{\partial c}{\partial r}\right) + P^{-2}\frac{\partial^2 c}{\partial z^2}\right\} \qquad \text{for } 1 < r < 1+\epsilon, \tag{2.8b}$$

in which $v(r) = V(R)/V_0$ is the dimensionless axial fluid velocity. The non-dimensional boundary and initial conditions are

$$\lambda\frac{\partial c}{\partial r}\bigg|_{r=1^+} = \frac{\partial c}{\partial r}\bigg|_{r=1^-}, \qquad c|_{r=1^+} = \beta c|_{r=1^-}, \qquad c|_{t=0} = \delta(z)\theta(1-r). \tag{2.9}$$

Following earlier workers (e.g. Aris 1956), we characterize tracer transport by calculating coefficients defined in terms of the axial moments of the tracer concentration. In order to do so, we define the dimensionless integrals, with respect to r and to both r and z respectively, over the fluid and wall phases by

$$\langle c\rangle^{(r)}(z,t) = 2\int_0^{1+\epsilon} c(r,z,t)r\,\mathrm{d}r, \qquad \langle c\rangle^{(r,z)}(t) = \int_{-\infty}^{\infty}\langle c\rangle^{(r)}(z,t)\,\mathrm{d}z. \tag{2.10}$$

The first of these can be split into a radial average over the fluid phase and a further integral, with the same normalization, over the wall phase: the normalization is such that $\langle c\rangle^{(r,z)} = 1$ initially. It is convenient also to define corresponding integrals $\langle\ldots\rangle_f^{(r,z)}$ and $\langle\ldots\rangle_w^{(r,z)}$ which are confined to fluid-phase and wall-layer contributions respectively.

The effective transport coefficients are defined in terms of the axial moments as follows. The fraction of tracer remaining in the system (i.e. including both fluid and wall phases) is

$$q(t) = \langle c\rangle^{(r,z)}(t). \tag{2.11}$$

Of course, for the impermeable outer boundary condition q is identically equal to 1. For the perfectly absorbing outer boundary condition, q stays close to 1 as long as the fraction of tracer reaching the outside of the wall layer remains small. The apparent convection velocity of tracer, defined as the rate of change of its mean axial position, is $V_0 u(t)$, where

$$u(t) = \frac{\mathrm{d}}{\mathrm{d}t}\left(\frac{\langle zc\rangle^{(r,z)}(t)}{\langle c\rangle^{(r,z)}(t)}\right). \tag{2.12}$$

The dispersion coefficient, defined as half the rate of change of the axial variance of the tracer distribution, is $Dk(t)$, where

$$k(t) = \tfrac{1}{2}P^2\frac{\mathrm{d}}{\mathrm{d}t}\left\{\frac{\langle z^2c\rangle^{(r,z)}(t)}{\langle c\rangle^{(r,z)}(t)} - \left(\frac{\langle zc\rangle^{(r,z)}(t)}{\langle c\rangle^{(r,z)}(t)}\right)^2\right\}. \tag{2.13}$$

We find below that the dependence of $k(t)$ on the Péclet number P can be expressed by writing $k(t) = P^2k_c(t) + k_d(t)$, in which the term containing k_c is the convective component of the dispersion coefficient and k_d is the diffusive component. The former corresponds to Taylor dispersion, and results from the distribution of tracer between regions of the system moving with different velocities (it is therefore strongly influenced by absorption by the stationary wall layer); the latter was simply equal to unity in Aris' (1956) treatment, but is now also modified by exchange between the phases.

Note that the integrals defined by (2.10), and consequently the resulting effective transport coefficients, differ from those used by Davidson & Schroter (1983), which were confined to the fluid phase. For purposes of comparison, we define analogous quantities q_f, u_f, k_{cf} and k_{df} in terms of integrals over the fluid phase alone.

2.2. *Solution for axial moments of concentration*

To solve for the transport coefficients q, u and k we apply to the tracer concentration a Laplace transform with respect to time and a Fourier transform with respect to axial distance. The combined effect of these two transforms is denoted by an overbar, viz.

$$\bar{c}(r,p,s) = \int_{-\infty}^{\infty}\int_{0}^{\infty} c(r,z,t)\exp(-st - \mathrm{i}pz)\mathrm{d}t\,\mathrm{d}z. \tag{2.14}$$

From (2.8*a*,*b*), the governing equations for $\bar{c}$ are

$$r^{-1}\frac{\partial}{\partial r}\left(r\frac{\partial\bar{c}}{\partial r}\right) = \{s + \mathrm{i}pv(r) + P^{-2}p^2\}\bar{c} - 1 \qquad \text{for } 0 \leqslant r < 1, \tag{2.15a}$$

$$r^{-1}\frac{\partial}{\partial r}\left(r\frac{\partial\bar{c}}{\partial r}\right) = \{\lambda^{-1}s + P^{-2}p^2\}\bar{c} \qquad \text{for } 1 < r < 1+\epsilon. \tag{2.15b}$$

The axial moments required to evaluate the transport coefficients from (2.11–2.13) may be deduced by calculating the first three terms of a series development of the form

$$\bar{c}(r,p,s) = \bar{c}_0(r,s) - \mathrm{i}p\bar{c}_1(r,s) - \tfrac{1}{2}p^2\{\bar{c}_{20}(r,s) + P^{-2}\bar{c}_{21}(r,s)\} + \ldots \tag{2.16}$$

(a similar small-p expansion of the axial Fourier transform was used by Lungu & Moffatt (1982) in their study of the fully developed dispersion of heat in a duct with a conducting wall); note that this expansion is valid for arbitrary P: in general

the coefficients are polynomials in P^{-2}. The required axial moments of tracer concentration are given in terms of radial integrals of these functions by

$$\left.\begin{aligned} \langle c\rangle^{(r,z)}(t) &= \langle c_0\rangle^{(r)}(t), \\ \langle zc\rangle^{(r,z)}(t) &= \langle c_1\rangle^{(r)}(t), \\ \langle z^2c\rangle^{(r,z)}(t) &= \langle c_{20}\rangle^{(r)}(t) + P^{-2}\langle c_{21}\rangle^{(r)}(t), \end{aligned}\right\} \tag{2.17}$$

where $\langle c_i\rangle^{(r)}(t)$ denotes the inverse Laplace transform of $\langle \bar{c}_i\rangle^{(r)}(s)$; equivalent equations relate the corresponding integrals of c over the fluid phase alone.

We obtain solutions for the integrals $\langle c_i\rangle^{(r)}$ for two different axial flow profiles. In the first case, Poiseuille flow, denoted by a superscript p, the flow profile is

$$v^{(p)}(r) = 2(1-r^2). \tag{2.18}$$

In the second case, in order to assess sensitivity to the flow profile, we repeat the calculation with a uniform axial flow, denoted by a superscript u, giving simply

$$v^{(u)}(r) = 1. \tag{2.19}$$

(Note that (2.15) can be solved exactly for $\bar{c}$ when the flow is uniform.)

The governing equations that apply to the functions $\bar{c}_i$ are obtained by substituting the series form (2.16) into equations (2.15). For $\bar{c}_0$, $\bar{c}_1$ and $\bar{c}_{20}$ the governing equations for $0 \leqslant r < 1$ are

$$r^{-1}\frac{\partial}{\partial r}\left(r\frac{\partial \bar{c}_0}{\partial r}\right) - s\bar{c}_0 = -1, \tag{2.20a}$$

$$r^{-1}\frac{\partial}{\partial r}\left(r\frac{\partial \bar{c}_1}{\partial r}\right) - s\bar{c}_1 = -v(r)\bar{c}_0, \tag{2.20b}$$

$$r^{-1}\frac{\partial}{\partial r}\left(r\frac{\partial \bar{c}_{20}}{\partial r}\right) - s\bar{c}_{20} = -2v(r)\bar{c}_1, \tag{2.20c}$$

and those for $1 < r < 1+\epsilon$ are

$$r^{-1}\frac{\partial}{\partial r}\left(r\frac{\partial \bar{c}_i}{\partial r}\right) - \lambda^{-1}s\bar{c}_i = 0 \qquad \text{for } i = 0, 1, 20. \tag{2.21}$$

Each $\bar{c}_i$ is regular at $r = 0$, and satisfies boundary conditions corresponding to those in (2.9) at the interface $r = 1$ and either (2.3) or (2.4) at $r = 1+\epsilon$. As a consequence of (2.9), the boundary conditions for these three functions at the outer boundary of the fluid can be expressed as

$$\left.\frac{\partial \bar{c}_i}{\partial r}\right|_{r=1^-} = -\kappa G s^{1/2}\bar{c}_i|_{r=1^-} \qquad \text{for } i = 0, 1, 20, \tag{2.22}$$

where

$$G(s) = -\lambda^{1/2}s^{-1/2}\left(\bar{c}_i^{-1}\frac{\partial \bar{c}_i}{\partial r}\right)\Bigg|_{r=1^+}. \tag{2.23}$$

By solving (2.21) for $\bar{c}_i$, $G(s)$ can be expressed explicitly in terms of modified Bessel functions.

By using (2.21) together with (2.23) and the interface conditions in (2.9), we find that for these three functions the fluid-phase integrals are related to the integrals over

both the fluid and wall phases by

$$\langle \bar{c}_i \rangle_f^{(r)} = \langle \bar{c}_i \rangle^{(r)} - 2\kappa G(1-H)s^{-1/2}\bar{c}_i|_{r=1^-} \qquad \text{for } i = 0, 1, 20, \tag{2.24}$$

where the function H is defined by

$$H(s) = (1+\epsilon)\left(\frac{\partial \bar{c}_i}{\partial r}\bigg|_{r=1^+}\right)^{-1} \frac{\partial \bar{c}_i}{\partial r}\bigg|_{r=1+\epsilon}. \tag{2.25}$$

Like $G(s)$, $H(s)$ can be expressed explicitly in terms of modified Bessel functions.

The situation is slightly more complicated for the function $\bar{c}_{21}$, owing to the effect of axial diffusion in the wall layer, which makes its first appearance at this order. The governing equations are

$$r^{-1}\frac{\partial}{\partial r}\left(r\frac{\partial \bar{c}_{21}}{\partial r}\right) - s\bar{c}_{21} = -2\bar{c}_0 \qquad \text{for } 0 \leqslant r < 1, \tag{2.26a}$$

$$r^{-1}\frac{\partial}{\partial r}\left(r\frac{\partial \bar{c}_{21}}{\partial r}\right) - \lambda^{-1}s\bar{c}_{21} = -2\bar{c}_0 \qquad \text{for } 1 < r < 1+\epsilon, \tag{2.26b}$$

with boundary conditions at $r = 0$ and $1+\epsilon$, and conditions at the interface $r = 1$, equivalent to those for the other $\bar{c}_i$. By differentiating (2.20a) and (2.21) with respect to s, we find that $\bar{c}_{21}$ can be expressed in terms of $\bar{c}_0$ and $\partial \bar{c}_0/\partial s$.

It is seen immediately from (2.20), (2.26) that $\bar{c}_0$ and $\bar{c}_{21}$ are independent of the fluid velocity profile. Explicit solutions for all the $\bar{c}_i$ can be obtained, and the required radial integrals evaluated, in terms of modified Bessel functions by a straightforward but lengthy procedure. Appendix A gives the resulting expressions for the quantities $\langle \bar{c}_i \rangle^{(r)}$ and $\bar{c}_i|_{r=1^-}$ for both Poiseuille and uniform flow. From these, expressions for $\langle \bar{c}_i \rangle_f^{(r)}$ can also be obtained using (2.24).

3. Asymptotic solution for a thin wall layer with a long diffusion timescale

3.1. *Assumptions*

The formulation of §2 makes no assumption about the relative sizes of the physical parameters governing the problem. The resulting solutions in Appendix A describe the time-development of the first three axial moments of tracer concentration for any values of the wall layer thickness h, and the ratios β, of tracer concentrations, and λ, of diffusion coefficients, across the wall layer–fluid interface. In principle these solutions for the Laplace transforms $\langle \bar{c}_i \rangle^{(r)}$ can be inverted in the form of infinite series to give the transport coefficients defined by (2.11)–(2.13), but the resulting expressions are impracticably complicated. Instead, in the remainder of the paper we consider the case where the wall layer thickness is thin compared with the radius of the tube, i.e. ϵ is asymptotically small, but the dimensionless quantity defined by

$$\ell = \epsilon\lambda^{-1/2} = hD^{1/2}/aD_w^{1/2} \tag{3.1}$$

is large. The square of this quantity represents the ratio of timescales for diffusion across the wall layer and the interior of the tube. Because this ratio is assumed to be large, the development of tracer transport takes place over two distinct timescales, the shorter of which is represented by the dimensionless time t defined in (2.7), and the longer by the rescaled variable

$$\tau = \ell^{-2}t = D_w T/h^2. \tag{3.2}$$

Our choice of parameters broadly follows Davidson & Schroter's (1983) study of gas transport and uptake in the bronchial tree. These essentially satisfy the assumptions above, since they have $\epsilon = 10^{-1}$ and $\lambda = 10^{-4}$, so that $\ell = 10$.

As stated above, we consider two possible boundary conditions at $r = 1 + \epsilon$, corresponding firstly to a boundary which is impermeable to tracer (2.3) and secondly to one which is perfectly absorbing (2.4). With the assumption that ϵ is small, the curvature of the wall layer can be neglected, and we find from (2.23) that

$$G(s) = \begin{cases} \tanh(\sigma^{1/2}) & \text{(impermeable)}, \\ \coth(\sigma^{1/2}) & \text{(perfectly absorbing)}, \end{cases} \tag{3.3}$$

in which

$$\sigma = \epsilon^2 \lambda^{-1} s = \ell^2 s \tag{3.4}$$

is a version of the Laplace transform variable rescaled to correspond to τ.

Similarly, from (2.25)

$$H(s) = \begin{cases} 0 & \text{(impermeable)} \\ \operatorname{sech}(\sigma^{1/2}) & \text{(perfectly absorbing).} \end{cases} \tag{3.5}$$

Since we assume that both ϵ and λ are small, axial diffusion of tracer in the wall layer, which by inspection of (A 1) results only in a small modification of k_d, can be neglected. In its absence, note also that $\bar{c}_1^{(u)} = \frac{1}{2}\bar{c}_{21}$; this means that the diffusive component of the dispersion coefficient, k_d, is equal to the apparent convection velocity due to uniform flow, $u^{(u)}$ (whether averages are based on the fluid phase alone, or on both phases). As a result the number of independent transport coefficients to be calculated is reduced: there are five in general, and for averages over both phases with the impermeable outer boundary condition there are only four, because $q = 1$.

With the assumptions above, in §3.2 we derive short-time approximations for the axial moments of tracer concentration, based on averages over both phases. Then, assuming also that κ is not as small as ℓ^{-3}, in §3.3 we derive approximate long-time solutions (the effect of this additional assumption is that the fully developed dispersion rate is dominated by exchange with, and diffusion within, the wall layer). The corresponding results for averages confined to the fluid phase are given in Appendix B.

3.2. *Short timescale*

On the short timescale, over which transport in the fluid phase develops, only an exponentially small quantity of tracer diffuses to the outside of the wall layer. As a result the leading-order short-time solution is the same whichever boundary condition is applied at this surface. In addition, since we assume that ϵ is small, the solution is also insensitive to the curvature of the wall layer. (In fact, since λ is also assumed small, even in the presence of a thick wall layer the curvature would remain negligible until a large time, of order λ^{-1}, had elapsed.)

The solution for the short timescale is most directly obtained by taking the limit $\lambda \to 0$ with s fixed in (3.3), (3.5). Provided that the real part of $s^{1/2}$ is positive, this gives $G \to 1$ and $H \to 0$. These values of G and H are therefore substituted into (A 1)–(A 4) and in the resulting expressions $s^{1/2}$ is defined by stipulating a branch cut along the negative real axis. The Laplace transforms are inverted by first subtracting out the parts that are singular as $s \to 0$ for separate inversion, then deforming the

contour of integration in the normal manner around the branch cut. This gives

$$\langle c_0\rangle^{(r)} = 1, \tag{3.6a}$$

$$\left\langle c_1^{(p)}\right\rangle^{(r)} = \pi^{-1/2}\kappa^{-1}t^{1/2} - \tfrac{1}{4}(\kappa^{-2} - \tfrac{2}{3}) + \pi^{-1}\kappa\int_0^\infty \left\{-8y^{-7/2}E^{-1}(y^{1/2}\mathscr{J} + 2\mathscr{J}')\mathscr{J}' + \tfrac{1}{2}\kappa^{-2}y^{-3/2}\right\}e^{-yt}dy, \tag{3.6b}$$

$$\left\langle c_1^{(u)}\right\rangle^{(r)} = \tfrac{1}{2}\langle c_{21}\rangle^{(r)} = \pi^{-1/2}\kappa^{-1}t^{1/2} - \tfrac{1}{4}(\kappa^{-2} - \tfrac{1}{2}) + \pi^{-1}\kappa\int_0^\infty \left(-2y^{-5/2}E^{-1}\mathscr{J}'^2 + \tfrac{1}{2}\kappa^{-2}y^{-3/2}\right)e^{-yt}dy, \tag{3.6c}$$

$$\left\langle c_{20}^{(p)}\right\rangle^{(r)} = \tfrac{1}{2}\kappa^{-2}t - \pi^{-1/2}(\kappa^{-3} - \tfrac{19}{24}\kappa^{-1})t^{1/2} + \tfrac{3}{8}(\kappa^{-4} - \tfrac{49}{36}\kappa^{-2} + \tfrac{7}{30}) + \pi^{-1}\kappa\int_0^\infty \left\{y^{-11/2}E^{-1}A_1^{(p)} + y^{-5}E^{-2}A_2^{(p)} - \tfrac{1}{2}(\kappa^{-4} - \tfrac{19}{24}\kappa^{-2})y^{-3/2}\right\}e^{-yt}dy, \tag{3.6d}$$

$$\left\langle c_{20}^{(u)}\right\rangle^{(r)} = \tfrac{1}{2}\kappa^{-2}t - \pi^{-1/2}(\kappa^{-3} - \tfrac{1}{2}\kappa^{-1})t^{1/2} + \tfrac{3}{8}(\kappa^{-4} - \kappa^{-2} + \tfrac{1}{9}) + \pi^{-1}\kappa\int_0^\infty \left\{y^{-7/2}E^{-1}A_1^{(u)} + y^{-3}E^{-2}A_2^{(u)} - \tfrac{1}{2}(\kappa^{-4} - \tfrac{1}{2}\kappa^{-2})y^{-3/2}\right\}e^{-yt}dy, \tag{3.6e}$$

in which

$$\mathscr{J} = J_0(y^{1/2}), \qquad \mathscr{J}' = J_0'(y^{1/2}), \qquad E = \kappa^2\mathscr{J}^2 + \mathscr{J}'^2, \tag{3.7}$$

where J_0 is the Bessel function of the first kind, and the functions $A_j^{(p,u)}$ are given by

$$A_1^{(p)} = 32\left\{2y\mathscr{J}^2 - \tfrac{1}{3}(y^{3/2} - 84y^{1/2})\mathscr{J}\mathscr{J}' - \tfrac{1}{3}(y^2 + 13y - 144)\mathscr{J}'^2\right\}, \tag{3.8a}$$

$$A_2^{(p)} = -\tfrac{32}{3}\left(-\kappa^2y^{3/2}\mathscr{J}^3 - 6\kappa^2y\mathscr{J}^2\mathscr{J}' + \{(1-2\kappa^2)y^{3/2} - 6\kappa^2y^{1/2}\}\mathscr{J}\mathscr{J}'^2 - 4\kappa^2(y+1)\mathscr{J}'^3\right)\mathscr{J}, \tag{3.8b}$$

$$A_1^{(u)} = 2\mathscr{J}'(y^{1/2}\mathscr{J} + 4\mathscr{J}'), \tag{3.8c}$$

$$A_2^{(u)} = 2\mathscr{J}\mathscr{J}'\left\{\kappa^2\mathscr{J}^2 - (1-2\kappa^2)\mathscr{J}'^2\right\}. \tag{3.8d}$$

The only parameter remaining in this short-time solution is the dimensionless absorption parameter κ. We can obtain simplified forms for special values of κ. When $\kappa = 0$, i.e. when the tracer is insoluble in the wall layer, we obtain by inverting (A 1), (A 4) the results

$$\left\langle c_1^{(p)}\right\rangle^{(r)} = \left\langle c_1^{(u)}\right\rangle^{(r)} = \tfrac{1}{2}\langle c_{21}\rangle^{(r)} = t, \tag{3.9a}$$

$$\left\langle c_{20}^{(p)}\right\rangle^{(r)} = t^2 + \tfrac{1}{24}t - \tfrac{1}{360} + 128\sum_{n=1}^{\infty} j_n'^{-8}e^{-j_n'^2t}, \tag{3.9b}$$

$$\left\langle c_{20}^{(u)}\right\rangle^{(r)} = t^2, \tag{3.9c}$$

in which j_n' is the nth (strictly) positive root of J_0'. Since no tracer enters the wall layer these results are the same as those based on the fluid phase alone. As is well

known, for this case the mean axial position of the tracer moves with the mean fluid velocity, and the diffusive component of the dispersion coefficient is as it would be in the absence of flow (i.e. unity). The linearly growing part of $\left\langle c_{20}^{(p)}\right\rangle^{(r)}$ represents Taylor dispersion, which is of course absent in the case of uniform flow.

If κ is considered to be non-zero but asymptotically small, the passage of tracer into the wall layer is very slow, giving rise to a new, long timescale, defined by

$$t_\kappa = \kappa^2 t. \tag{3.10}$$

The dominant contributions to the integrals (3.6) are from a neighbourhood of the lower limit of integration, of size κ^{-2}. Evaluating these contributions we obtain

$$\left\langle c_1^{(p)}\right\rangle^{(r)} \sim \left\langle c_1^{(u)}\right\rangle^{(r)} \sim \tfrac{1}{2}\langle c_{21}\rangle^{(r)} = \tfrac{1}{4}\pi^{-1/2}\kappa^{-2}\left(4t_\kappa^{1/2} - \pi^{1/2} + \mathrm{e}^{4t_\kappa}\Gamma\right) + O(1), \tag{3.11a}$$

$$\left\langle c_{20}^{(p)}\right\rangle^{(r)} \sim \left\langle c_{20}^{(u)}\right\rangle^{(r)} = \tfrac{1}{8}\pi^{-1/2}\kappa^{-4}\left(4\pi^{1/2}t_\kappa - 12t_\kappa^{1/2} + 3\pi^{1/2} + (8t_\kappa - 3)\mathrm{e}^{4t_\kappa}\Gamma\right) + O(\kappa^{-2}), \tag{3.11b}$$

in which $\Gamma \equiv \Gamma(\frac{1}{2}, 4t_\kappa)$ in the notation of Abramowitz & Stegun (1972). In this approximation the results simplify, being expressible in terms of a set of universal functions, with the κ-dependence reducing to a stretching of both the timescale and the axial lengthscale by a factor κ^{-2}. These universal functions are also independent of the assumed flow profile. However, the usefulness of these small-κ approximations is somewhat limited, since the short-time solution is valid only up to times of order ℓ^2 (or λ^{-1} if the wall layer is very thick). Therefore in practice the approximations given by (3.11) will be relevant only when $\ell^{-1} \ll \kappa \ll 1$ (or $\lambda^{1/2} \ll \kappa \ll 1$ for a thick wall layer).

Finally, the case of infinite κ corresponds to perfect absorption of tracer by the wall layer (with no desorption into the fluid phase). The solution may be found, either directly, or by evaluating the contributions to the integrals in (3.6) from the narrow peaks in the integrands that occur near the roots of $\mathscr{J}$ when κ is large. This gives

$$\left\langle c_1^{(p)}\right\rangle^{(r)} = \tfrac{1}{6} - 32\sum_{n=1}^{\infty} j_n^{-6}\mathrm{e}^{-j_n^2 t}, \tag{3.12a}$$

$$\left\langle c_1^{(u)}\right\rangle^{(r)} = \tfrac{1}{2}\langle c_{21}\rangle^{(r)} = \tfrac{1}{8} - 4\sum_{n=1}^{\infty} j_n^{-4}\mathrm{e}^{-j_n^2 t}, \tag{3.12b}$$

$$\left\langle c_{20}^{(p)}\right\rangle^{(r)} = \tfrac{7}{80} - \tfrac{256}{3}\sum_{n=1}^{\infty}\left\{j_n^{-6}(1 + j_n^{-2})t + \tfrac{13}{2}j_n^{-8}(1 - \tfrac{62}{13}j_n^{-2})\right\}\mathrm{e}^{-j_n^2 t}, \tag{3.12c}$$

$$\left\langle c_{20}^{(u)}\right\rangle^{(r)} = \tfrac{1}{24} - 8\sum_{n=1}^{\infty}(j_n^{-4}t + j_n^{-6})\mathrm{e}^{-j_n^2 t}, \tag{3.12d}$$

where j_n is the nth positive root of J_0. Note that, just as the small-κ limit is not a uniform one, the infinite-κ results do not provide a uniformly valid approximation to the large-κ behaviour as a function of time. Physically, this is because for finite κ, no matter how large, tracer is desorbed into the fluid phase after its initial absorption; when κ is infinite, however, the axial position of absorbed tracer is effectively fixed for all time.

3.3. *Long timescale*

As stated above, we assume that the dimensionless quantity ℓ defined by (3.1) is asymptotically large, so that that tracer molecules typically take much longer to diffuse across the wall layer than across the interior of the tube. The rescaled long-time variable reflecting this timescale is τ, defined by (3.2). We therefore seek a solution on this timescale by fixing τ while assuming $\ell \gg 1$. In order to avoid implying that nearly all the tracer passes into the wall layer, we also assume that the parameter defined by

$$\mu = \kappa\ell \,(= \epsilon\beta) \tag{3.13}$$

is fixed during the $\ell \to \infty$ process. This means that the solution remains valid when the equilibrium fractions of tracer in the fluid phase and the wall phase are comparable. Detailed consideration shows that the resulting approximation retains its validity for large values of μ, but breaks down when μ is small, of order ℓ^{-2} or less, when the wall layer no longer dominates tracer transport. Thus, it is not applicable when κ drops to values comparable with, or less than, ℓ^{-3}. For example, for the impermeable outer boundary condition, the neglect of dispersion in the fluid phase can be shown to underestimate the fully developed value of $k_c^{(p)}$ by approximately $\frac{1}{32}\kappa^{-1}\ell^{-3}$ relative to its true value.

The solution for the long timescale is obtained by considering the rescaled versions of the Laplace transform inversion integrals for the axial moments, namely

$$\langle c_i\rangle^{(r,z)}(\ell^2\tau) = (2\pi\mathrm{i})^{-1}\ell^{-2}\int_{\mathscr{C}} \langle \bar{c}_i\rangle^{(r)}(\ell^{-2}\sigma)\mathrm{e}^{\sigma\tau}\mathrm{d}\sigma, \tag{3.14}$$

where $\mathscr{C}$ is, as usual, a contour in the complex plane passing to the right of the singularities of the integrand. The poles of the Laplace-transformed moments lie along the negative real axis. To obtain the long-time solution, for which τ is fixed and $\ell \gg 1$, it is sufficient to consider values of σ of order unity (larger values give exponentially small contributions). Thus we require a small-s form of the Laplace transform; specifically the form for $s = \ell^{-2}\sigma$, with $\ell \gg 1$ and σ fixed. This must be inverted with respect to σ and multiplied by ℓ^{-2}.

It is straightforward to expand the general solutions to obtain the required asymptotic forms. From (A 1)–(A 4), we find

$$\ell^{-2}\langle \bar{c}_0\rangle^{(r)} = \frac{\sigma^{1/2} + 2\mu G(1-H)}{\sigma(\sigma^{1/2} + 2\mu G)} + O(\ell^{-2}), \tag{3.15a}$$

$$\ell^{-2}\left\langle \bar{c}_1^{(p)}\right\rangle^{(r)} \sim \ell^{-2}\left\langle \bar{c}_1^{(u)}\right\rangle^{(r)} \sim \tfrac{1}{2}\ell^{-2}\langle \bar{c}_{21}\rangle^{(r)} = \ell^2\frac{\sigma^{1/2} + 2\mu G(1-H)}{\sigma^{3/2}(\sigma^{1/2} + 2\mu G)^2} + O(1), \tag{3.15b}$$

$$\ell^{-2}\left\langle \bar{c}_{20}^{(p)}\right\rangle^{(r)} \sim \ell^{-2}\left\langle \bar{c}_{20}^{(u)}\right\rangle^{(r)} = \ell^4\frac{2(\sigma^{1/2} + 2\mu G(1-H))}{\sigma^2(\sigma^{1/2} + 2\mu G)^3} + O(\ell^2). \tag{3.15c}$$

From (2.24) we deduce that the fluid-phase averages are obtained by setting $H = 1$ in these equations (see Appendix B). By inspection of (3.15), at leading order the long-time approximations for all three moments are independent of the assumed flow profile; physically, this is because radial diffusion in the wall is the rate-limiting transport process. Also, for large σ, $G \to 1$ and $H \to 0$ for both the impermeable and perfectly absorbing outer boundary conditions. Thus, as we should expect physically, the solutions for both cases converge for small values of τ, when only a small amount of tracer has had time to reach the outer boundary.

In each case, the leading term of the Laplace transform is regular apart from an

infinite series of poles along the negative real axis of the σ-plane. Evaluating the residues in the normal manner we obtain, firstly for the impermeable outer boundary condition,

$$\langle c_0\rangle^{(r)} = 1, \tag{3.16a}$$

$$\left\langle c_1^{(p)}\right\rangle^{(r)} \sim \left\langle c_1^{(u)}\right\rangle^{(r)} \sim \tfrac{1}{2}\langle c_{21}\rangle^{(r)} = \ell^2\left(\frac{\tau}{1+2\mu}+\frac{2\mu}{3(1+2\mu)^2}-2\sum_{n=1}^{\infty}a_n^{-2}f_n^{-1}\mathrm{e}^{-a_n^2\tau}\right)+O(1), \tag{3.16b}$$

$$\left\langle c_{20}^{(p)}\right\rangle^{(r)} \sim \left\langle c_{20}^{(u)}\right\rangle^{(r)} = \ell^4\left(\frac{\tau^2}{(1+2\mu)^2}+\frac{8\mu\tau}{3(1+2\mu)^3}+\frac{8\mu(\mu-2)}{15(1+2\mu)^4}\right.$$
$$\left.-8\sum_{n=1}^{\infty}(\tau+\tfrac{3}{2}a_n^{-2}-f_n^{-1}\sec^2 a_n)a_n^{-2}f_n^{-2}\mathrm{e}^{-a_n^2\tau}\right)+O(\ell^2), \tag{3.16c}$$

as $\ell\to\infty$ with μ and τ fixed, in which

$$f_n = 1+2\mu\sec^2 a_n, \tag{3.17}$$

and a_n is the nth (strictly) positive root of the equation

$$a_n\cos a_n + 2\mu\sin a_n = 0. \tag{3.18}$$

The results for the perfectly absorbing outer boundary condition are

$$\langle c_0\rangle^{(r)} = 4\mu\sum_{n=0}^{\infty}b_n^{-1}g_n^{-1}\mathrm{cosec}b_n\,\mathrm{e}^{-b_n^2\tau}+O(\ell^{-2}), \tag{3.19a}$$

$$\left\langle c_1^{(p)}\right\rangle^{(r)} \sim \left\langle c_1^{(u)}\right\rangle^{(r)} \sim \tfrac{1}{2}\langle c_{21}\rangle^{(r)} = 8\ell^2\sum_{n=0}^{\infty}\left\{\mu[\tau+b_n^{-2}]\mathrm{cosec}b_n-\tfrac{1}{4}b_n^{-1}g_n\right.$$
$$\left.+\tfrac{1}{4}g_n^{-1}(1-2\mu\mathrm{cosec}^2 b_n)\mathrm{cosec}b_n\right\}b_n^{-1}g_n^{-2}\mathrm{e}^{-b_n^2\tau}+O(1), \tag{3.19b}$$

$$\left\langle c_{20}^{(p)}\right\rangle^{(r)} \sim \left\langle c_{20}^{(u)}\right\rangle^{(r)} = 16\ell^4\sum_{n=0}^{\infty}\left\{\mu[\tau^2+\tfrac{5}{2}b_n^{-2}\tau+3b_n^{-4}]\mathrm{cosec}b_n\right.$$
$$+\tfrac{1}{2}[\tau+\tfrac{3}{2}b_n^{-2}][g_n^{-1}(1-4\mu\mathrm{cosec}^2 b_n)\mathrm{cosec}b_n-b_n^{-1}g_n]$$
$$+\tfrac{1}{2}b_n^{-1}\mathrm{cosec}^2 b_n+\tfrac{1}{4}\mu b_n^{-2}g_n^{-2}[-1+2\mathrm{cosec}^2 b_n+16\mu\mathrm{cosec}^2 b_n-16\mu\mathrm{cosec}^4 b_n$$
$$\left.-12\mu^2\mathrm{cosec}^4 b_n+8\mu^2\mathrm{cosec}^6 b_n]\mathrm{cosec}b_n\right\}b_n^{-1}g_n^{-3}\mathrm{e}^{-b_n^2\tau}+O(\ell^2), \tag{3.19c}$$

as $\ell\to\infty$ with μ and τ fixed, in which

$$g_n = 1+2\mu\mathrm{cosec}^2 b_n, \tag{3.20}$$

and b_n is the nth positive root of the equation

$$b_n\sin b_n - 2\mu\cos b_n = 0. \tag{3.21}$$

The effective transport coefficients at long times, unlike those at short times, depend on the dimensionless quantity ℓ in addition to the dimensionless absorption

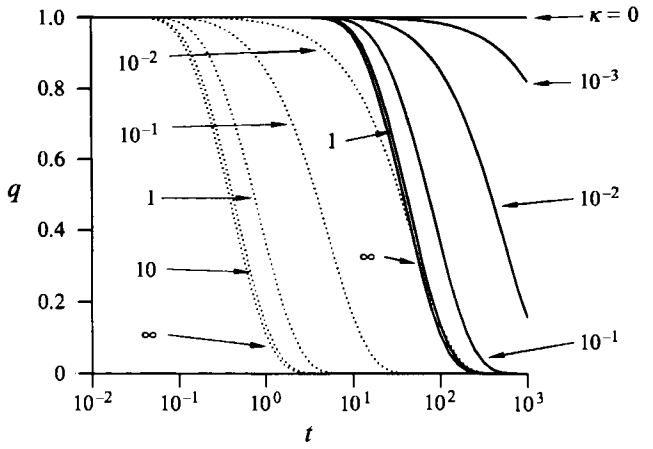

FIGURE 1. The fraction of tracer remaining in the system, q, calculated from the long-time approximation (3.19) for the perfectly absorbing outer boundary condition: for $\ell = 10$ (———), with $\kappa = 0, 10^{-3}, 10^{-2}, 10^{-1}, 1$ and ∞; and for $\ell = 1$ (·····), with $\kappa = 0, 10^{-2}, 10^{-1}, 1, 10$ and ∞.

parameter κ. However, given the fact that the timescale is proportional to ℓ^2, the solution essentially depends only on the single parameter $\mu = \kappa\ell$.

4. Results

4.1. *The fraction of tracer remaining in the system, and in the fluid phase*

The simplest transport coefficients are q, the fraction of tracer remaining in the system (including the wall layer), and q_f, the fraction remaining in the fluid phase alone, which are calculated by solving the two-dimensional diffusion equation governing $\bar{c}_0$ in §2.2 (and are therefore independent of the flow profile assumed). The numerical results for these two coefficients provide a convenient illustration of the asymptotic structure of the solution, with its two distinct timescales.

Figure 1 shows the time-dependence of q. On the short timescale, and for the impermeable boundary condition at all times, q is equal to unity. The long-time results for the perfectly absorbing outer boundary condition are shown in figure 1 for a range of values of κ, with $\ell = 1$ and 10. In every case q decreases monotonically towards zero with increasing time, and the onset of the decrease indicates the transition from the short- to the long-time régime. Comparison of the solutions for $\ell = 1$ and 10 illustrates how the long-time approximations scale with ℓ. As demonstrated in §3.3, they belong to a single family of curves, whose timescales are proportional to ℓ^2, and which are parametrized by $\mu = \kappa\ell$, so that different curves having the same shape correspond to values of κ that are inversely proportional to ℓ. Note the sensitivity to ℓ implied by these scalings: e.g. a change in wall layer thickness by a factor of 10 would change the timescale by two orders of magnitude. Most of the results presented below are for $\ell = 10$, which illustrates the separation of timescales and also permits comparison with the numerical results of Davidson & Schroter (1983).

For the fraction of tracer remaining in the fluid phase, q_f, because tracer begins to move into the wall layer immediately there is a non-trivial variation on the short as well as the long timescale. Figure 2 shows q_f as a function of time when $\kappa = 10^{-1}$. The short-time solution, which depends only on κ, is shown together with long-time solutions for four different values of ℓ, for both impermeable and perfectly

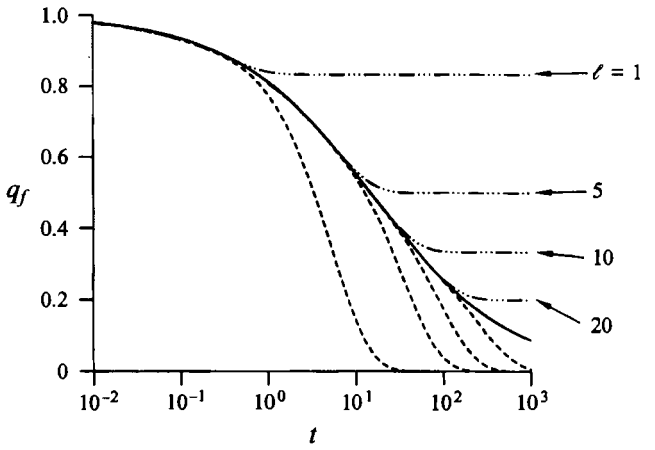

FIGURE 2. The fraction of tracer remaining in the fluid phase, q_f, for $\kappa = 10^{-1}$. The short-time solution (———), calculated from (B1), is shown together with long-time solutions (— · · —, impermeable outer boundary condition; – – – –, perfectly absorbing outer boundary condition), calculated from (B5), (B6), for four values of ℓ: 1,5,10 and 20. For each value of ℓ, both long-time solutions diverge from the short-time solution at around the same time.

absorbing outer boundary conditions. As is always so, the long-time solutions for both conditions merge with each other as t decreases below ℓ^2, and then match very smoothly to the short-time solution. For q_f, although the asymptotic expansions used are strictly only valid for $\ell \gg 1$, in practice they give reasonably accurate results even when $\ell = 1$. Comparison with figure 1 shows that matching with the short-time solutions occurs later for the fluid-based coefficient than for that based on both phases. This is because the integrals based on both phases begin to change when molecules have diffused from the inner to the outer boundary of the wall layer, but the fluid-phase integrals are not affected until molecules have diffused back to the inner boundary again. Therefore molecules are required to diffuse twice the distance to affect the fluid-phase average, and since the time for diffusion scales as the square of the distance, the transition is later by roughly a factor of four. This scaling is borne out by the results shown both here and below. At long times, for the perfectly absorbing outer boundary condition, q_f tends to zero as all the tracer moves out of the fluid phase. However, for the impermeable outer boundary condition, an equilibrium partition between the phases is approached, with q_f tending to $(1 + 2\kappa\ell)^{-1}$ in the long-time approximation.

Figure 3 illustrates the behaviour of q_f for a range of values of κ. Here we show the short-time solution, and for $\kappa \leqslant 1$ the long-time solutions for both outer boundary conditions when $\ell = 10$ (for larger values of κ, by the time the large-t solution becomes valid, q_f is too small to be clearly seen). As for the other transport coefficients shown below, provided κ is not too large the long-time solutions are a good approximation throughout the range of time, matching with the short-time curves slightly earlier when κ is larger. Note that the results for $\kappa = 10$ differ little from those for infinite κ. In the latter case uptake by the wall layer is extremely rapid, with 99% of tracer having left the fluid phase by $t = 0.74$.

4.2. *Transport coefficients based on fluid-phase averages*

We consider next the behaviour of transport coefficients based on moments of the axial concentration distribution in the fluid phase alone, as used by previous workers

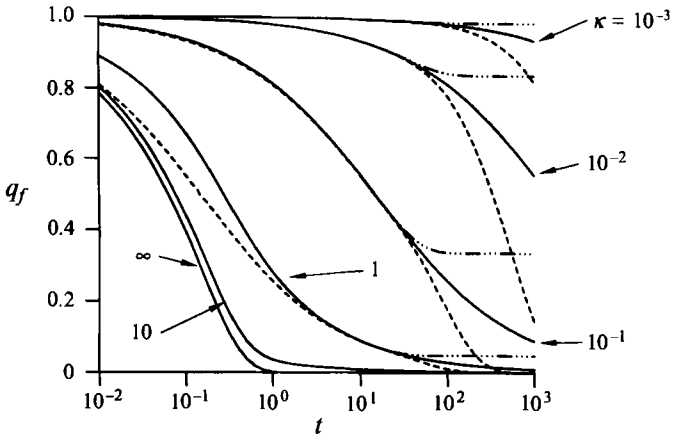

FIGURE 3. The fraction of tracer remaining in the fluid phase, q_f, for $\kappa = 10^{-3}, 10^{-2}, 10^{-1}, 1, 10$ and ∞. The short-time solutions (———), calculated from (B1), (B4), are shown, and for the cases with $\kappa \leqslant 1$ we also show long-time solutions (— · · —, impermeable outer boundary condition; – – – – perfectly absorbing outer boundary condition), calculated from (B5), (B6), for $\ell = 10$. Below about $t = 10$, each pair of long-time solutions coincides, and for clarity only the perfectly absorbing case is shown.

(Davidson & Schroter 1983). Figure 4 shows the apparent convection velocity due to Poiseuille flow, based on fluid-phase averages, $u_f^{(p)}$, for a range of values of κ. There is close agreement between the combined short-time and long-time (impermeable outer boundary condition) results and the corresponding curves shown in figure 3 of Davidson & Schroter (1983), in which the pronounced 'kinks' correspond to the transition between the short- and long-time solutions, when the influence of the outer boundary of the wall layer becomes important. The relationship between the short- and long-time solutions is similar to that in figure 3, with close agreement for smaller κ, but divergence for larger κ. Unlike the short-time approximation (in which all the tracer is eventually taken up by the stationary wall layer), each of the long-time solutions tends to a positive limit as $t \to \infty$. For the impermeable outer boundary condition, the limit is equal to the limiting fraction of tracer in the fluid phase, i.e. $(1 + 2\kappa\ell)^{-1}$ in this approximation. The limiting value for the perfectly absorbing boundary condition, $2g_0^{-1}$, is larger: because of removal at the outside of the wall layer, proportionately more of the tracer remaining in the system lies in the moving fluid (cf. Lungu & Moffatt 1982).

Other features of the predictions reflect the fact that $u_f^{(p)}$ is based on moments of concentration in the fluid phase only, and thus, in effect, is calculated for different sets of tracer molecules at different times. For example, at short times $u_f^{(p)}$ rises above unity, i.e. the apparent convection velocity for tracer is larger than the average flow velocity. This is because, in the early stages, tracer molecules in the slower-moving fluid near the wall layer are moving out of the fluid phase and thus leaving the averages. The average position is progressively dominated by molecules near the tube axis, where the flow is fastest (cf. Davidson & Schroter 1983). The initial rise of $u_f^{(p)}$ is followed by a dramatic fall before $t = 1$. This is due to the desorption from the wall layer of tracer absorbed earlier, which brings back into the averages molecules that have been delayed while in the wall layer, whereas those that have spent longer in the fluid phase, and have thus been convected furthest, continue to be absorbed and to leave the averages. The resulting decrease in $u_f^{(p)}$ is stronger for larger κ, and

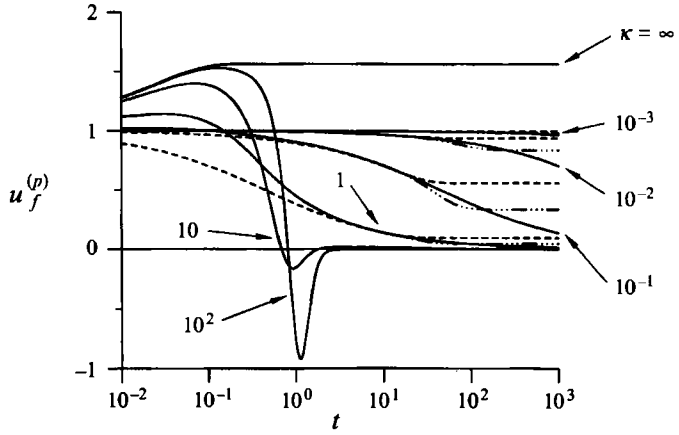

FIGURE 4. The apparent convection velocity due to Poiseuille flow, based on fluid-phase averages, $u_f^{(p)}$, for $\kappa = 10^{-3}, 10^{-2}, 10^{-1}, 1, 10, 10^2$ and ∞. The short-time solutions (———), calculated from (B1), are shown, and for the cases with $\kappa \leqslant 1$ we also show long-time solutions (——·——, impermeable outer boundary condition; – – – –, perfectly absorbing outer boundary condition), calculated from (B5), (B6), for $\ell = 10$. Below about $t = 10$, each pair of long-time solutions coincides, and for clarity only the perfectly absorbing case is shown.

when $\kappa = 10$ it is actually sufficient to make $u_f^{(p)}$ negative for a short period around $t = 1$. The case of infinite κ is singular in the sense that tracer is never desorbed from the wall layer, so that there is no tendency for $u_f^{(p)}$ to decrease; instead, it increases monotonically to a limiting value greater than unity, with an exponentially decreasing amount of tracer remaining in the fluid phase, and the highest concentration at the axis of the tube, where the fluid velocity is highest.

Many of the same features are present in the results (not shown) for the effective dispersion coefficients, $k_{cf}^{(p)}$ and k_{df}. Once again, for higher κ, both these coefficients, like $u_f^{(p)}$, become negative just before $t = 1$. In each case the reason is similar to that described above: tracer absorbed earlier, which has not spread axially while in the wall layer, re-enters the fluid phase, while the more dispersed tracer still in the fluid phase continues to be absorbed; for sufficiently high κ, this actually reduces both components of the axial spread of the tracer in the fluid phase.

4.3. *Transport coefficients based on averages over both phases (Poiseuille flow)*

The paradoxical behaviour described in §4.2, resulting from the use of fluid-phase-based averages of tracer concentration, suggests that tracer transport will be more reasonably described by coefficients defined in terms of both fluid- and wall-layer concentrations. This means that for the impermeable outer boundary condition the effective transport coefficients reflect the movement of all the tracer molecules initially released, rather than expressing a mixture of axial transport and effects of exchange between the phases. For the perfectly absorbing outer boundary condition, although tracer does leave the averages, it does not subsequently re-enter, so that paradoxical behaviour is minimized by including the contribution of the wall layer. Implications for comparison with experiment are discussed in §5.

Figure 5 illustrates the apparent convection velocity due to Poiseuille flow based on averages including both phases, $u^{(p)}$, for a range of values of κ, with long-time results for both impermeable and perfectly absorbing boundary conditions. In contrast to the paradoxical behaviour in figure 4, for the impermeable outer boundary

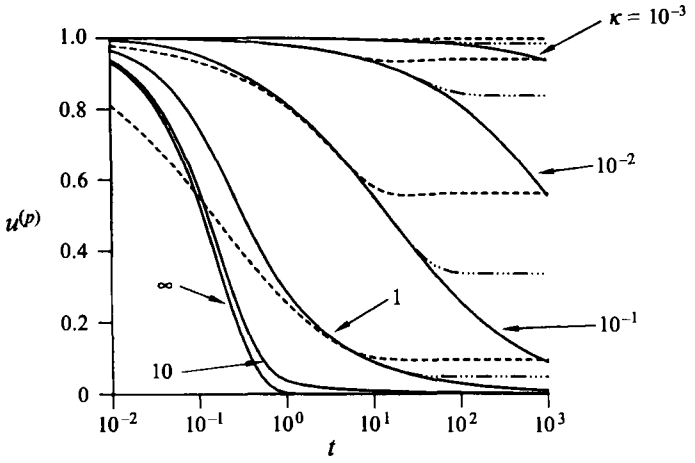

FIGURE 5. The apparent convection velocity due to Poiseuille flow, based on averages over both phases, $u^{(p)}$, for $\kappa = 10^{-3}, 10^{-2}, 10^{-1}, 1, 10$ and ∞. The short-time solutions (———), calculated from (3.6), are shown, and for the cases with $\kappa \leqslant 1$ we also show long-time solutions (— · · —, impermeable outer boundary condition; – – – –, perfectly absorbing outer boundary condition), calculated from (3.16), (3.19), for $\ell = 10$. Below about $t = 10$, each pair of long-time solutions coincides, and for clarity only the perfectly absorbing case is shown.

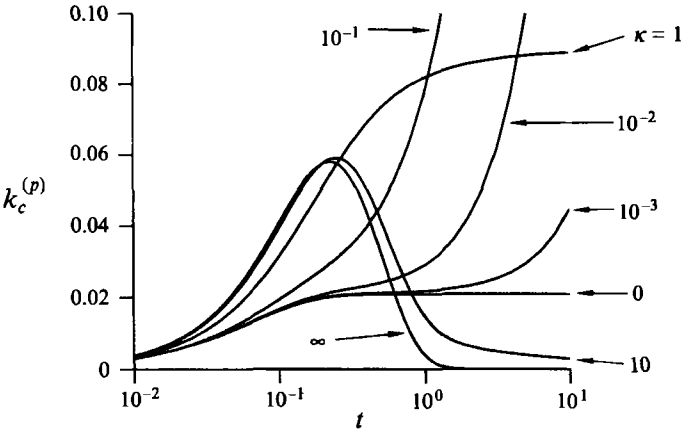

FIGURE 6. The convective component of the dispersion coefficient due to Poiseuille flow, based on averages over both phases, $k_c^{(p)}$, for $\kappa = 0, 10^{-3}, 10^{-2}, 10^{-1}, 1, 10$ and ∞. Only the short-time solutions, calculated from (3.6), are shown.

condition $u^{(p)}$ decreases monotonically with time. For the perfectly absorbing outer boundary condition, when κ is small there remains a barely visible minimum near the transition to the long-time régime, probably due to a much weaker version of the effects discussed in §4.2. Also, the large-κ solutions now approach the infinite-κ curve without exhibiting the large deviations shown in figure 4. Other aspects of the solutions are qualitatively as discussed in §4.2. In particular, the long-time limit of the apparent convection velocity for the impermeable outer boundary condition is the same as that based on the fluid phase alone, and as before is smaller than that for the perfectly absorbing outer boundary condition.

Figure 6 shows results for the convective component of the dispersion coefficient due to Poiseuille flow, based on averages over both phases, $k_c^{(p)}$, in the short-time

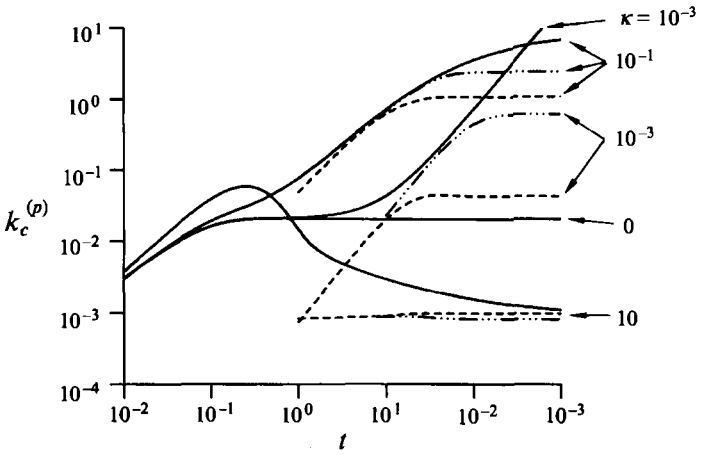

FIGURE 7. The convective component of the dispersion coefficient due to Poiseuille flow, based on averages over both phases, $k_c^{(p)}$. Log-log plot for moderate κ (0,10^{-3},10^{-1} and 10), to show short-time solutions (———), calculated from (3.6), together with long-time solutions (— · · — impermeable outer boundary condition; – – – – perfectly absorbing outer boundary condition), calculated from (3.16), (3.19), for $\ell = 10$. Below about $t = 10$, each pair of long-time solutions coincides, and for clarity only the perfectly absorbing case is shown.

approximation only. The $\kappa = 0$ curve shows the time-development of Taylor dispersion (as calculated by Gill & Sankarasubramanian 1970). For all values of κ greater than zero, the short-time solution increases from zero initially to reach a maximum, then decreases towards zero again for long times, as all the tracer tends to enter the stationary wall layer. For small values of κ, the curves are given approximately by a stretched version of a universal solution (3.11), with a long timescale and a large rate of dispersion, both proportional to κ^{-2}. The long timescale represents the slowness of tracer movement into the wall layer when κ is small. (Note that this small-κ approximation is only relevant in practice if its timescale is shorter than that of the long-time solution, which reflects the time taken to diffuse across the wall layer, i.e. if $1 \ll \kappa^{-1} \ll \ell$. In terms of dimensional parameters this requirement could be satisfied, for example, for a given wall layer thickness if $D_w/D \to 0$ and $\beta \to \infty$ with $\beta^2 D_w/D \ll 1$.)

The relationship of the short-time behaviour of $k_c^{(p)}$ with the long-time solutions is shown in figure 7, as a logarithmic plot. Both the long-time solutions tend to constant values as $t \to \infty$. For the impermeable outer boundary condition, the limiting value is the same as that based on fluid-phase averages (cf. Davidson & Schroter 1983). When κ is small, this is higher than for the perfectly absorbing outer boundary condition, whereas for higher κ, as shown by the $\kappa = 10$ curve, the opposite is true. This behaviour can be understood qualitatively as follows. In general, the convective component of dispersion arises from the distribution of tracer between parts of the system moving with different velocities; for the cases shown, the important aspect of this distribution is the partition between the stationary wall layer and the moving fluid phase. The resulting dispersion rate is greatest at some point intermediate between the two extreme cases in which all the tracer lies in one phase or the other. For example, for the impermeable outer boundary condition in this approximation it is easily shown that the large-t limit of $k_c^{(p)}$ is maximized when $\mu = \frac{1}{4}$, which corresponds to two thirds of the tracer being in the fluid phase. On the one hand, when κ is small, $k_c^{(p)}$ is lower for the perfectly absorbing outer boundary condition, because only a

small fraction of the tracer is in the wall layer, and absorption lowers this fraction still further, moving the system further away from the optimal partition between the two phases. This effect is reinforced because the tracer being absorbed at the outer boundary of the wall layer lies predominantly to the rear of the rest, tending to reduce further the axial spread. But on the other hand, for higher values of κ, most of the tracer lies in the wall layer. This means that $k_c^{(p)}$ is much smaller for both outer boundary conditions, but now the perfectly absorbing condition moves the system closer to the optimal partition and gives a larger rate of dispersion than in the impermeable case.

Another respect in which figure 7 differs from the results already discussed is that the long-time approximations are less accurate for shorter times. The close agreement at small values of κ noted for q_f and $u^{(p)}$ is absent (although the discrepancy is accentuated by the logarithmic plot). This is because for small κ the short-time variation is dominated by the tracer remaining in the fluid phase, and is therefore highly dependent on the flow profile, whereas the leading-order long-time approximations reflect the evolution of wall-layer concentrations. The continuation of these approximations to shorter times accordingly fails to agree closely with the Poiseuille-flow results (although they do match closely the results for a uniform flow profile, shown below in figure 10). For the smallest value of κ considered, the long-time solution becomes inaccurate even at longer times because, as discussed in §3.3, transport in the wall layer ceases to dominate even the long-time behaviour when $\kappa\ell^3$ drops to order unity.

As noted in §3.1, the results for the diffusive component of the dispersion coefficient, k_d, are identical to those for the apparent convection velocity due to uniform flow, $u^{(u)}$ (shown in figure 8 below). In every respect the behaviour of k_d is qualitatively similar to that of the apparent convection velocity, $u^{(p)}$ (shown in figure 5), because the dispersive action of axial diffusion is analogous to the convective action of flow.

4.4. *Transport coefficients based on a uniform flow profile*

Finally, we examine the sensitivity of our results to the flow profile by comparing the values calculated above for Poiseuille flow with those obtained when the fluid moves with a uniform axial velocity. As already noted, the fraction of tracer remaining in the system, q, and the diffusive component of the dispersion coefficient, k_d, are independent of the flow profile assumed. In addition, the apparent convection velocity for uniform flow, $u^{(u)}$, is numerically equal to k_d. Moreover, as shown in §3.3, the long-time solutions are independent of the flow profile, at leading order, for every coefficient.

Figure 8 shows the comparison of the apparent convection velocities $u^{(p)}$ and $u^{(u)}$, due to Poiseuille and uniform flow profiles, demonstrating the difference in tracer convection due to the two flow profiles when the total flow rates are the same. For each value of κ the two short-time solutions are shown, together with the long-time solutions, which are common to both flow profiles. When κ is not too large, there is close agreement between the two curves throughout the range of time, although $u^{(p)}$ is a little larger than $u^{(u)}$ due to the lowering of concentration near the interface, which for Poiseuille flow is a slower-moving region. For $\kappa = 10^{-1}$, the difference between $u^{(p)}$ and $u^{(u)}$ is always less than about 0.02, i.e. the apparent convection velocities differ by less than 2% of the average fluid velocity. The long-time curves match smoothly to the short-time results for both profiles; in fact when κ is small, comparison with figure 5 shows that the long-time results and the uniform-flow curve lie very close to each other at all times. For larger κ the difference between $u^{(p)}$ and $u^{(u)}$ is greater

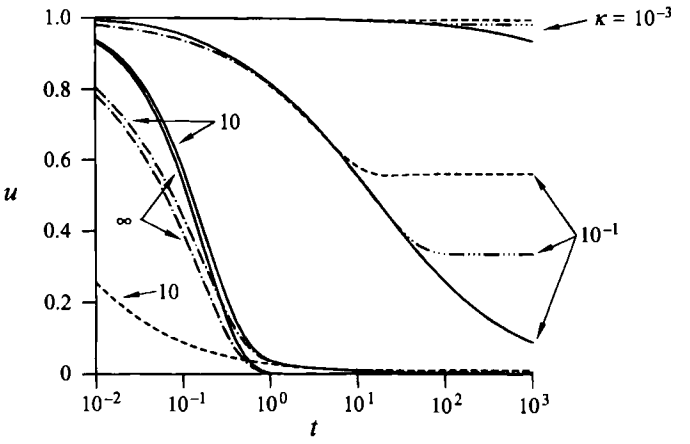

FIGURE 8. The apparent convection velocity, based on averages over both phases: comparison of results for Poiseuille flow ($u^{(p)}$) and uniform flow ($u^{(u)}$). Curves are shown for $\kappa = 10^{-3}, 10^{-1}, 10$ and ∞. The short-time solutions (———, Poiseuille flow; — · —, uniform flow), calculated from (3.6), are shown, and for the cases with finite κ we also show long-time solutions (— · · —, impermeable outer boundary condition; – – – –, perfectly absorbing outer boundary condition), calculated from (3.16), (3.19), for $\ell = 10$ (these are independent of the axial flow profile assumed; they are shown for $t \geqslant 1$ when $\kappa \leqslant 10^{-1}$, with the perfectly absorbing case shown for the whole range of time when $\kappa = 10$).

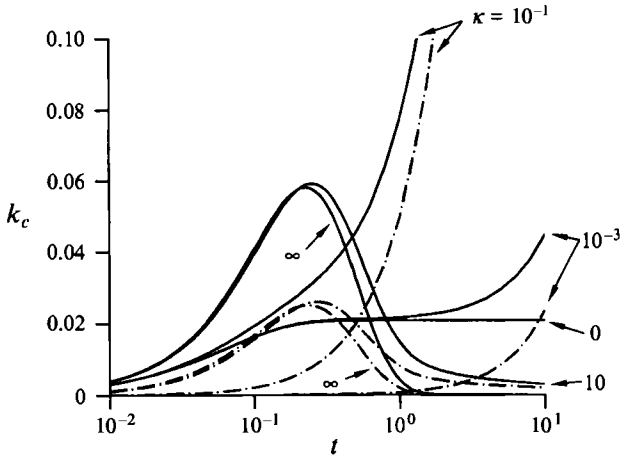

FIGURE 9. The convective component of the dispersion coefficient, based on averages over both phases: comparison of results for Poiseuille flow ($k_c^{(p)}$———) and uniform flow ($k_c^{(u)}$— · —). Curves are shown for $\kappa = 0, 10^{-3}, 10^{-1}, 10$ and ∞. Only the short-time solutions, calculated from (3.6), are shown.

(and the close agreement between the long-time and the uniform-flow results is lost). Note, however, that even when κ is infinite, the results for the two flow profiles merge by $t \approx 1$. Thus, at worst the apparent convection velocity depends significantly on the flow profile only in the earliest stages, and for a wide range of κ it is virtually insensitive to the flow field.

In Figs 9 and 10 we show results for the convective components of the dispersion coefficient, $k_c^{(p)}$ and $k_c^{(u)}$, for Poiseuille and uniform flow profiles. In figure 9, the short-time results are shown up to $t = 10$ for a range of values of κ. At early times, when transport in the fluid phase is dominant, $k_c^{(u)}$ is much smaller than $k_c^{(p)}$; indeed,

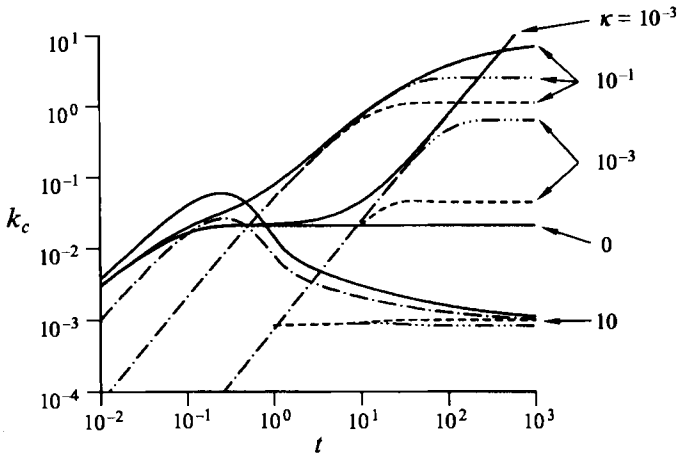

FIGURE 10. The convective component of the dispersion coefficient, based on averages over both phases: comparison of results for Poiseuille flow ($k_c^{(p)}$) and uniform flow ($k_c^{(u)}$). Log-log plot for moderate κ (0,10^{-3},10^{-1} and 10), to show short-time solutions (——— Poiseuille flow; ·—·— uniform flow), calculated from (3.6), together with long-time solutions (—···— impermeable outer boundary condition; – – – – perfectly absorbing outer boundary condition), calculated from (3.16), (3.19), for $\ell = 10$ (these are independent of the axial flow profile assumed; they are shown for $t \geqslant 10$ when $\kappa = 10^{-3}$ and for $t \geqslant 1$ when $\kappa \geqslant 10^{-1}$).

when $\kappa = 0$, $k_c^{(u)}$ is zero. For small, non-zero κ, however, at longer times both $k_c^{(u)}$ and $k_c^{(p)}$ tend to equality with the universal solution, given by (3.11), whose timescale and magnitude are both large and of order κ^{-2}. For larger values of κ, $k_c^{(u)}$ reaches a peak at about the same time as $k_c^{(p)}$, but with roughly half the magnitude, with the two curves tending to equality at longer times, though not as rapidly as the apparent convection velocities shown in figure 8.

In figure 10 the short-time solutions for $k_c^{(p)}$ and $k_c^{(u)}$, together with the long-time solutions (common to both flow profiles), are shown as a logarithmic plot, for a range of values of κ. Provided κ is not too large, the long-time solutions merge smoothly with the short-time uniform-flow curves (but not, as noted above, those for Poiseuille flow). The comparison of predictions for k_c based on the two flow profiles can be summarized as follows. On the one hand, when κ is large, in the period when dispersion is fastest transport in the fluid phase is important, so the predictions based on the two profiles differ significantly, but at longer times they decrease towards a common limit. On the other, when κ is small (i.e. comparable with ℓ^{-3}), transport in the fluid phase is important in determining k_c even at long times, so that neither the short-time results for uniform flow nor the long-time results are expected to approximate the true solution for Poiseuille flow. For intermediate values of κ, however, $k_c^{(u)}$ differs from $k_c^{(p)}$ by an amount that is always small compared with the fully developed value. For example, for $\kappa = 10^{-1}$ the error incurred by the uniform-flow approximation is always less than about 3% of the limiting value as $t \to \infty$.

5. Discussion

In this section we draw from our results some general conclusions, which we expect to be applicable, at least qualitatively, to a wide range of systems in which transport by convection and diffusion in a fluid phase is combined with exchange with a

stationary phase in which diffusion is much slower. The central feature revealed by the analysis is that, as a consequence of the assumption that $\ell = hD^{1/2}/aD_w^{1/2} \gg 1$, the development of dispersion takes place over two widely separated timescales, for each of which the mathematical solution can be approximated by a simplified form. The shorter timescale, a^2/D, reflects the time taken for tracer molecules to diffuse across the fluid phase, and is the same as for the development of Taylor dispersion. During this stage, at leading order, the influence of the wall layer is fully characterized by the single dimensionless parameter, $\kappa = (D_w/D)^{1/2}\beta$; the thickness of the wall layer, and the prevailing conditions at its outer boundary, do not affect the solution. The second, much longer, timescale, h^2/D_w, reflects the time for tracer to diffuse across the wall layer. Unless uptake is very small, on this timescale transport is characterized by the single dimensionless parameter $\mu = \beta h/a$, implying that, at leading order, transport is unaffected by the form of the fluid flow profile, and depends on flow only through the cross-sectionally averaged fluid velocity. In dimensional terms, the requirement for this to be true is that $\beta \gg a^3 D_w/h^3 D$, which with $D_w \ll D$ is a much weaker condition than $\beta h \gg a$: thus tracer diffusion in the wall layer can be rate-determining even if only a relatively small fraction of the tracer is within the wall layer at any time.

An important conclusion is that if, as in Davidson & Schroter's (1983) analysis, transport coefficients are calculated on the basis of fluid-phase concentrations alone, they behave in a complicated and paradoxical manner, and even become temporarily negative if uptake is sufficiently large (§4.2). The parameter range where this is possible includes, for example, gases of interest to lung toxicologists, for which the value of β can be as high as 1500 (for ethanol). Assuming D_w/D is roughly 10^{-4}, this would imply $\kappa = 15$, which is within the range where the fluid-phase-based coefficients behave paradoxically. This behaviour can be avoided if tracer within the wall layer is also taken into account. Clearly, for purposes of comparison with experiment, the nature of the measurements determines which of the two methods is appropriate. If one measures the instantaneous spatial concentration distribution in the fluid phase alone, fluid-phase averages are obviously required. Similarly, averages over both phases are appropriate for comparison with measurements of the spatial distribution within both phases. However, in many experiments what is actually measured is the time-varying concentration at a fixed position in the system. Moreover, in modelling any transport problem in a branching network of tubes the same problem arises. For example, to model gas transport and uptake in the bronchial tree during inspiration, we require not the axial distribution in an infinitely long tube, but the response as a function of time at fixed positions in each airway (including the efflux from its distal end) resulting from a specified time-varying influx at the proximal end. One of our main conclusions, as discussed below, is that such measurements cannot be compared with predictions derived from either choice of spatial averages. In particular, it is evident that a negative effective velocity could never be observed by making concentration measurements at fixed positions within this system.

A comparison of the results based on Poiseuille flow with those based on a hypothetical uniform flow profile shows that, in many cases, the transport characteristics are relatively insensitive to the flow profile. For example, provided uptake is not too large (say for $\kappa \leqslant 10^{-1}$), the two values of the apparent tracer convection velocity differ by only a few per cent of the mean fluid velocity. For the dispersion coefficient, the situation is more complicated because, as stated above, when κ is very small transport is dominated by convection in the fluid phase, which means that k_c is sensitive to the flow profile. However, for moderate values of κ (e.g. $\kappa = 10^{-1}$) the differences between the results for the two flow profiles amount to only a few per

cent of the fully developed value. We conclude that in many circumstances tracer transport is relatively insensitive to the details of the axial flow field. Of course, in many circumstances the flow field will include components transverse to the axis of the tube (e.g. in developing flow, or in the presence of curvature or bifurcations). Our results suggest that these transverse components will affect only the short-time development of dispersion (which in any case is sensitive to the initial radial concentration distribution (Aris 1956)), and that the long-time solution calculated here will still apply. Indeed, for fully developed dispersion in a curved tube with a wall layer like the one considered here, the recent numerical calculations of Jayaraman, Pedley & Goyal (1995) have directly demonstrated that the departure from Poiseuille flow has only a small effect.

When interpreting the results presented above, it must be borne in mind that they contain information only about axial moments of the tracer distribution. The method of moments has been widely used, because in addition to having a clear physical interpretation, at long times the moments specify the asymptotic form of the axial concentration distribution, which is a translating, spreading and decaying Gaussian (cf. Lungu & Moffatt 1982). However, at shorter times, the concentration is not approximately Gaussian, and the information presented by the moments is far less comprehensive. The timescale for the development of the Gaussian form can be increased by orders of magnitude in the presence of a wall layer in which the tracer is soluble, causing the tracer distribution to be extremely skewed, with a long tail at the rear due to tracer having been delayed by the wall layer (see (5.1) below). The difficulty is exacerbated because, as discussed above, it is often desirable to know the time-variation of concentration at a fixed point rather than its spatial variation at a fixed time. If the concentration distribution is non-Gaussian, there is no straightforward equivalence between the two.

The implications for transport in the lung can be illustrated by comparing the time for passage through an individual airway with that required for the development of dispersion. For an insoluble tracer, the convective component of the dispersion coefficient reaches 95% of its fully developed value by the dimensionless time $t \approx 0.2$. We can use the recent geometrical analysis of the bronchial tree by Phillips, Kaye & Schroter (1994) to estimate the values of t based on the average times for inspired air to pass through individual airways, assuming a steady rate of inspiration of $20\,\mathrm{l\,min^{-1}}$ and a diffusion coefficient of $10^{-1}\,\mathrm{cm^2 s^{-1}}$. The value of t estimated in this way reaches 0.2 only in airways of diameter 3.5 mm or less. This means that, even for an insoluble tracer, dispersion cannot be considered to be fully developed in the several hundred largest conducting airways. For soluble tracers, the timescale for development is much larger, of the order of ℓ^2. In Davidson & Schroter's model $\ell = 10$, which indicates a requirement that $t \approx 100$ or more, implying that dispersion is not fully developed in any of the conducting airways of the lung.

A simple example which illustrates both the departure from a Gaussian spatial distribution and the dramatic difference between moments based on space- and time-variation can be provided by considering the solution for a uniform flow profile, for times that are long, but not sufficiently long that the outer boundary of the wall layer has an influence. The resulting approximation is

$$c(r, z, t) \sim \pi^{-1/2} \kappa z t^{-3/2} \exp(-\kappa^2 z^2 t^{-1}) \tag{5.1}$$

for $1 \ll t \sim z^2 \ll \ell^2$, or in dimensional terms, $a^2/D \ll T \sim DZ^2/V_0^2 a^2 \ll h^2/D_w$. Viewed as a function of z, this is clearly far from Gaussian, but has well-defined moments whose rates of change agree with the large-t form of the (fluid-phase based)

short-time results given in Appendix B(§B.1). These moments reflect a distribution whose lengthscale is proportional to $\kappa^{-1}t^{1/2}$. However, viewed as a function of time at fixed position, not only is the concentration non-Gaussian, but the integrals for all the moments of time, except the zeroth, diverge. This means that the mean and variance of the downstream concentration distribution as a function of time are infinite. It is only the fact that this approximation breaks down at longer times, when the influence of the outer boundary is felt, that enables us to define these quantities meaningfully. This simple example demonstrates that, in the presence of a wall layer, in practical terms the standard dispersion formulation gives very little information about the temporal concentration distribution which can actually be measured.

C.G.P. is supported by a research fellowship from the Wellcome Trust, and S.R.K. by the Leverhulme Trust. The authors are grateful to Dr K. H. Parker and other colleagues for helpful comments and suggestions on the manuscript.

Appendix A. General solution

The functions required to calculate axial moments of tracer concentration, $\bar{c}_i$ (for $i = 0, 1$ and 20), satisfy the governing equations (2.20) in the fluid phase, subject to the boundary conditions (2.22) at the interface with the wall layer; the solution for the remaining function, $\bar{c}_{21}$, can be expressed in terms of these functions and their s-derivatives. Solutions for the $\bar{c}_i$, and expressions for the quantities G and H defined by (2.23) and (2.25), can be derived explicitly in terms of modified Bessel functions.

After lengthy manipulation, the following expressions for the required averages are obtained:

$$\langle \bar{c}_0 \rangle^{(r)} = -2\kappa GHs^{-1/2}\bar{c}_0|_{r=1^-} + s^{-1}, \tag{A 1a}$$

$$\left\langle \bar{c}_1^{(p)} \right\rangle^{(r)} = -2\kappa GHs^{-1/2}\bar{c}_1^{(p)}|_{r=1^-} + s^{-2} - 8\kappa Gs^{-7/2}\Delta^{-1}(s^{1/2}\mathscr{I} - 2\mathscr{I}'), \tag{A 1b}$$

$$\left\langle \bar{c}_1^{(u)} \right\rangle^{(r)} = -2\kappa GHs^{-1/2}\bar{c}_1^{(u)}|_{r=1^-} + s^{-1}\langle \bar{c}_0 \rangle_f^{(r)}, \tag{A 1c}$$

$$\begin{aligned}\left\langle \bar{c}_{20}^{(p)} \right\rangle^{(r)} &= -2\kappa GHs^{-1/2}\bar{c}_{20}^{(p)}|_{r=1^-} + \tfrac{8}{3}s^{-5}(s^2 - 6s - 48) \\ &\quad + 64s^{-9/2}\Delta^{-1}\mathscr{I} - \tfrac{32}{3}\kappa Gs^{-7/2}\Delta^{-2}\mathscr{I}^2 \\ &\quad + \tfrac{32}{3}\kappa Gs^{-11/2}\Delta^{-1}\left\{(s^{3/2} + 84s^{1/2})\mathscr{I} + (s^2 - 13s - 144)\mathscr{I}'\right\} \\ &\quad - 32\kappa^2 G^2 s^{-5}\Delta^{-2}\left\{s\mathscr{I}^2 + \tfrac{1}{3}(s^{3/2} - 3s^{1/2})\mathscr{I}\mathscr{I}' - \tfrac{2}{3}(s-1)\mathscr{I}'^2\right\},\end{aligned} \tag{A 1d}$$

$$\begin{aligned}\left\langle \bar{c}_{20}^{(u)} \right\rangle^{(r)} &= -2\kappa GHs^{-1/2}\bar{c}_{20}^{(u)}|_{r=1^-} + 2s^{-3} + 2\kappa Gs^{-7/2}\Delta^{-1}(s^{1/2}\mathscr{I} - 4\mathscr{I}') \\ &\quad - 2\kappa Gs^{-3}\Delta^{-2}\mathscr{I}\mathscr{I}' - 2\kappa^2 G^2 s^{-3}\Delta^{-2}\mathscr{I}'^2,\end{aligned} \tag{A 1e}$$

$$\begin{aligned}\langle \bar{c}_{21} \rangle^{(r)} &= -2\kappa GHs^{-1/2}\bar{c}_{21}|_{r=1^-} + 2s^{-1}\langle \bar{c}_0 \rangle_f^{(r)} \\ &\quad + 2\lambda\left(s^{-1}\langle \bar{c}_0 \rangle_w^{(r)} + 2\kappa s^{-1}\frac{\partial}{\partial s}(GHs^{1/2})\bar{c}_0|_{r=1^-}\right),\end{aligned} \tag{A 1f}$$

in which

$$\mathscr{I} = I_0(s^{1/2}), \qquad \mathscr{I}' = I_0'(s^{1/2}), \qquad \Delta = \kappa G\mathscr{I} + \mathscr{I}', \tag{A 2}$$

where I_0 is a modified Bessel function, G is given by (3.3), H by (3.5), the fluid-phase

and wall-phase integrals of $\bar{c}_0$ are

$$\left.\begin{aligned}\langle\bar{c}_0\rangle_f^{(r)} &= s^{-1} - 2\kappa G s^{-3/2}\Delta^{-1}\mathscr{F}',\\ \langle\bar{c}_0\rangle_w^{(r)} &= 2\kappa G(1-H)s^{-3/2}\Delta^{-1}\mathscr{F}'\end{aligned}\right\} \tag{A 3}$$

and the values $\bar{c}_i|_{r=1^-}$ are

$$\bar{c}_0|_{r=1^-} = s^{-1}\Delta^{-1}\mathscr{F}', \tag{A 4a}$$

$$\bar{c}_1^{(p)}|_{r=1^-} = 4s^{-3}\Delta^{-1}(s^{1/2}\mathscr{F} - 2\mathscr{F}') - \tfrac{2}{3}\kappa G s^{-5/2}\Delta^{-2}\left\{s\mathscr{F}^2 - s^{1/2}\mathscr{F}\mathscr{F}' - (s-1)\mathscr{F}'^2\right\}, \tag{A 4b}$$

$$\bar{c}_1^{(u)}|_{r=1^-} = s^{-2}\Delta^{-1}\mathscr{F}' - \tfrac{1}{2}\kappa G s^{-3/2}\Delta^{-2}(\mathscr{F}^2 - \mathscr{F}'^2), \tag{A 4c}$$

$$\begin{aligned}\bar{c}_{20}^{(p)}|_{r=1^-} = {} & \tfrac{16}{3}s^{-3}\Delta^{-2}\mathscr{F}^2 - \tfrac{8}{9}\kappa G s^{-2}\Delta^{-3}\mathscr{F}^3\\ & - \tfrac{16}{3}s^{-5}\Delta^{-1}\left\{(s^{3/2} + 60s^{1/2})\mathscr{F} + (s^2 - 13s - 120)\mathscr{F}'\right\}\\ & + \tfrac{4}{45}\kappa G s^{-9/2}\Delta^{-2}\left\{9(s^2 + \tfrac{67}{3}s)\mathscr{F}^2 + 10(s^{5/2} + \tfrac{33}{5}s^{3/2} - \tfrac{132}{5}s^{1/2})\mathscr{F}\mathscr{F}'\right.\\ & \left. + (s^2 - 133s + 204)\mathscr{F}'^2\right\}\\ & - \tfrac{16}{9}\kappa^2 G^2 s^{-4}\Delta^{-3}\left\{s^{3/2}\mathscr{F}^3 + (s^2 - \tfrac{3}{2}s)\mathscr{F}^2\mathscr{F}' - (s^{3/2} - s^{1/2})\mathscr{F}\mathscr{F}'^2 - \tfrac{1}{2}(s-1)^2\mathscr{F}'^3\right\},\end{aligned} \tag{A 4d}$$

$$\begin{aligned}\bar{c}_{20}^{(u)}|_{r=1^-} = {} & s^{-3}\Delta^{-1}(s^{1/2}\mathscr{F} + 2\mathscr{F}') - s^{-5/2}\Delta^{-2}\mathscr{F}\mathscr{F}'\\ & - \tfrac{1}{2}\kappa G s^{-5/2}\Delta^{-2}(4\mathscr{F}^2 - s^{1/2}\mathscr{F}\mathscr{F}' - 3\mathscr{F}'^2)\\ & - \tfrac{1}{2}\kappa G s^{-2}\Delta^{-3}\mathscr{F}^3 - \kappa^2 G^2 s^{-2}\Delta^{-3}(\mathscr{F}^2 - \tfrac{1}{2}\mathscr{F}'^2)\mathscr{F}',\end{aligned} \tag{A 4e}$$

$$\bar{c}_{21}|_{r=1^-} = 2\bar{c}_1^{(u)}|_{r=1^-} + 2\lambda\kappa s^{-3/2}\Delta^{-2}\mathscr{F}\mathscr{F}'\frac{\partial}{\partial s}(Gs^{1/2}). \tag{A 4f}$$

Appendix B. Solutions for integrals based on the fluid phase only

B.1. *Short-time solution*

The solutions corresponding to (3.6)–(3.8), but for moments based on integration over the fluid phase alone, are

$$\langle c_0\rangle_f^{(r)} = 2\pi^{-1}\kappa\int_0^\infty y^{-3/2}E^{-1}\mathscr{F}'^2 e^{-yt}dy, \tag{B 1a}$$

$$\begin{aligned}\left\langle c_1^{(p)}\right\rangle_f^{(r)} = {} & \tfrac{1}{4}\kappa^{-2} - 8\pi^{-1}\kappa\int_0^\infty\left(2y^{-7/2}E^{-1}(y^{1/2}\mathscr{F} + 2\mathscr{F}')\mathscr{F}'\right.\\ & \left. + \tfrac{1}{3}\kappa^2 y^{-3}E^{-2}\left\{y\mathscr{F}^2 + y^{1/2}\mathscr{F}\mathscr{F}' + (y+1)\mathscr{F}'^2\right\}\mathscr{F}\mathscr{F}'\right)e^{-yt}dy,\end{aligned} \tag{B 1b}$$

$$\begin{aligned}\left\langle c_1^{(u)}\right\rangle_f^{(r)} = \tfrac{1}{2}\langle c_{21}\rangle_f^{(r)} = {} & \tfrac{1}{4}\kappa^{-2} - 2\pi^{-1}\kappa\int_0^\infty\left\{2y^{-5/2}E^{-1}\mathscr{F}'^2\right.\\ & \left. + \kappa^2 y^{-2}E^{-2}(\mathscr{F}^2 + \mathscr{F}'^2)\mathscr{F}\mathscr{F}'\right\}e^{-yt}dy,\end{aligned} \tag{B 1c}$$

$$\left\langle c_{20}^{(p)}\right\rangle_f^{(r)} = \tfrac{1}{2}\pi^{-1/2}\kappa^{-3}t^{1/2} - \tfrac{3}{8}(\kappa^{-4} - \tfrac{3}{4}\kappa^{-2}) + \pi^{-1}\kappa\int_0^\infty \Big\{ y^{-11/2}E^{-1}A_{f1}^{(p)} + y^{-5}E^{-2}A_{f2}^{(p)} + \kappa^2 y^{-9/2}E^{-3}A_{f3}^{(p)} + \tfrac{1}{4}\kappa^{-4}y^{-3/2}\Big\}\mathrm{e}^{-yt}\mathrm{d}y, \tag{B 1d}$$

$$\left\langle c_{20}^{(u)}\right\rangle_f^{(r)} = \tfrac{1}{2}\pi^{-1/2}\kappa^{-3}t^{1/2} - \tfrac{3}{8}(\kappa^{-4} - \tfrac{1}{2}\kappa^{-2}) + \pi^{-1}\kappa\int_0^\infty \Big\{ 12y^{-7/2}E^{-1}\mathscr{F}'^2 + \kappa^2 y^{-3}E^{-2}A_{f2}^{(u)} + \kappa^2 y^{-5/2}E^{-3}A_{f3}^{(u)} + \tfrac{1}{4}\kappa^{-4}y^{-3/2}\Big\}\mathrm{e}^{-yt}\mathrm{d}y, \tag{B 1e}$$

where

$$A_{f1}^{(p)} = 64\left\{ y\mathscr{F}^2 - \tfrac{1}{3}(y^{3/2} - 72y^{1/2})\mathscr{F}\mathscr{F}' - \tfrac{1}{3}(y^2 + 13y - 132)\mathscr{F}'^2\right\}, \tag{B 2a}$$

$$A_{f2}^{(p)} = -\tfrac{64}{3}y^{3/2}\mathscr{F}^2\mathscr{F}'^2 - 16\kappa^2\Big\{-\tfrac{4}{3}y^{3/2}\mathscr{F}^4 + \tfrac{1}{5}(y^2 - \tfrac{127}{3}y)\mathscr{F}^3\mathscr{F}' + \tfrac{2}{9}(y^{5/2} - \tfrac{63}{5}y^{3/2} - \tfrac{222}{5}y^{1/2})\mathscr{F}^2\mathscr{F}'^2 - \tfrac{1}{45}(y^2 + 253y + 324)\mathscr{F}\mathscr{F}'^3\Big\}, \tag{B 2b}$$

$$A_{f3}^{(p)} = \tfrac{32}{9}\Big\{ y^{3/2}\mathscr{F}^3 + (y^2 + \tfrac{3}{2}y)\mathscr{F}^2\mathscr{F}' + (y^{3/2} + y^{1/2})\mathscr{F}\mathscr{F}'^2 + \tfrac{1}{2}(y+1)^2\mathscr{F}'^3\Big\}(3\kappa^2\mathscr{F}^2 - \mathscr{F}'^2)\mathscr{F}' + \tfrac{16}{9}y^2(\kappa^2\mathscr{F}^2 - 3\mathscr{F}'^2)\mathscr{F}^4, \tag{B 2c}$$

$$A_{f2}^{(u)} = 2(4\mathscr{F}^2 - y^{1/2}\mathscr{F}\mathscr{F}' + 5\mathscr{F}'^2)\mathscr{F}\mathscr{F}', \tag{B 2d}$$

$$A_{f3}^{(u)} = (\kappa^2\mathscr{F}^2 - 3\mathscr{F}'^2)\mathscr{F}^4 + (2\mathscr{F}^2 + \mathscr{F}'^2)(3\kappa^2\mathscr{F}^2 - \mathscr{F}'^2)\mathscr{F}'^2. \tag{B 2e}$$

When κ is small, the equations corresponding to (3.11) are

$$\langle c_0\rangle_f^{(r)} = \pi^{-1/2}\mathrm{e}^{4t_\kappa}\Gamma + O(\kappa^2), \tag{B 3a}$$

$$\left\langle c_1^{(p)}\right\rangle_f^{(r)} \sim \left\langle c_1^{(u)}\right\rangle_f^{(r)} \sim \tfrac{1}{2}\langle c_{21}\rangle_f^{(r)} = \tfrac{1}{4}\pi^{-1/2}\kappa^{-2}\left(-4t_\kappa^{1/2} + \pi^{1/2} + (8t_\kappa - 1)\mathrm{e}^{4t_\kappa}\Gamma\right) + O(1), \tag{B 3b}$$

$$\left\langle c_{20}^{(p)}\right\rangle_f^{(r)} \sim \left\langle c_{20}^{(u)}\right\rangle_f^{(r)} = \tfrac{3}{8}\pi^{-1/2}\kappa^{-4}\left(-\tfrac{16}{3}t_\kappa^{3/2} + 4t_\kappa^{1/2} - \pi^{1/2} + (\tfrac{32}{3}t_\kappa^2 - 4t_\kappa + 1)\mathrm{e}^{4t_\kappa}\Gamma\right) + O(\kappa^{-2}). \tag{B 3c}$$

The results corresponding to (3.12), for infinite κ, are

$$\langle c_0\rangle_f^{(r)} = 4\sum_{n=1}^{\infty} j_n^{-2}\mathrm{e}^{-j_n^2 t}, \tag{B 4a}$$

$$\left\langle c_1^{(p)}\right\rangle_f^{(r)} = \tfrac{16}{3}\sum_{n=1}^{\infty}\left\{ j_n^{-2}(1 + j_n^{-2})t + \tfrac{3}{2}j_n^{-4}(1 - 6j_n^{-2})\right\}\mathrm{e}^{-j_n^2 t}, \tag{B 4b}$$

$$\left\langle c_1^{(u)}\right\rangle_f^{(r)} = \tfrac{1}{2}\langle c_{21}\rangle_f^{(r)} = t\langle c_0\rangle_f^{(r)}, \tag{B 4c}$$

$$\left\langle c_{20}^{(p)}\right\rangle_f^{(r)} = \tfrac{64}{9}\sum_{n=1}^{\infty}\Big\{j_n^{-2}(1+j_n^{-2})^2t^2 + \tfrac{29}{10}j_n^{-4}(1-\tfrac{133}{29}j_n^{-2}-\tfrac{234}{29}j_n^{-4})t$$
$$+\tfrac{7}{2}j_n^{-6}(1-\tfrac{267}{7}j_n^{-2}+\tfrac{1310}{7}j_n^{-4})\Big\}\mathrm{e}^{-j_n^2t}, \tag{B 4d}$$

$$\left\langle c_{20}^{(u)}\right\rangle_f^{(r)} = t^2\langle c_0\rangle_f^{(r)}. \tag{B 4e}$$

Note the particularly simple form taken by the uniform-profile results. The apparent convection velocity $u_f^{(u)}$ is unity, the convective component of the dispersion coefficient is zero, and the diffusive component is unity. These simplifications arise because when κ is infinite no tracer re-enters the fluid phase after absorption.

B.2. *Long-time solution*

The solutions corresponding to (3.16), (3.19), but for moments based on integration over the fluid phase alone, are, for the impermeable outer boundary condition,

$$\langle c_0\rangle_f^{(r)} = (1+2\mu)^{-1} + 2\sum_{n=1}^{\infty} f_n^{-1}\mathrm{e}^{-a_n^2\tau} + O(\ell^{-2}), \tag{B 5a}$$

$$\left\langle c_1^{(p)}\right\rangle_f^{(r)} \sim \left\langle c_1^{(u)}\right\rangle_f^{(r)} \sim \tfrac{1}{2}\langle c_{21}\rangle_f^{(r)} = \ell^2\left(\frac{\tau}{(1+2\mu)^2} + \frac{4\mu}{3(1+2\mu)^3}\right.$$
$$\left.+4\sum_{n=1}^{\infty}\left\{\tau + \tfrac{1}{2}a_n^{-2} - f_n^{-1}\sec^2 a_n\right\} f_n^{-2}\mathrm{e}^{-a_n^2\tau}\right) + O(1), \tag{B 5b}$$

$$\left\langle c_{20}^{(p)}\right\rangle_f^{(r)} \sim \left\langle c_{20}^{(u)}\right\rangle_f^{(r)} = \ell^4\left(\frac{\tau^2}{(1+2\mu)^3} + \frac{4\mu\tau}{(1+2\mu)^4} + \frac{8(4\mu-3)\mu}{15(1+2\mu)^5}\right.$$
$$+8\sum_{n=1}^{\infty}\Big\{\tau^2 + \tfrac{3}{2}a_n^{-2}\tau + \tfrac{3}{2}a_n^{-4} - 3f_n^{-1}[\tau + a_n^{-2}]\sec^2 a_n \tag{B 5c}$$
$$\left.+\mu a_n^{-2}f_n^{-2}[2 - 3\sec^2 a_n - 8\mu\sec^2 a_n + 6\mu\sec^4 a_n]\sec^2 a_n\Big\} f_n^{-3}\mathrm{e}^{-a_n^2\tau}\right)$$
$$+O(\ell^2), \tag{B 5d}$$

and for the perfectly absorbing outer boundary condition,

$$\langle c_0\rangle_f^{(r)} = 2\sum_{n=0}^{\infty} g_n^{-1}\mathrm{e}^{-b_n^2\tau} + O(\ell^{-2}), \tag{B 6a}$$

$$\left\langle c_1^{(p)}\right\rangle_f^{(r)} \sim \left\langle c_1^{(u)}\right\rangle_f^{(r)} \sim \tfrac{1}{2}\langle c_{21}\rangle_f^{(r)}$$
$$= 4\ell^2\sum_{n=0}^{\infty}\left\{\tau + \tfrac{1}{2}b_n^{-2} - g_n^{-1}\mathrm{cosec}^2 b_n\right\} g_n^{-2}\mathrm{e}^{-b_n^2\tau} + O(1), \tag{B 6b}$$

$$\left\langle c_{20}^{(p)}\right\rangle_f^{(r)} \sim \left\langle c_{20}^{(u)}\right\rangle_f^{(r)} = 8\ell^4 \sum_{n=0}^{\infty}\Big\{\tau^2 + \tfrac{3}{2}b_n^{-2}\tau + \tfrac{3}{2}b_n^{-4} - 3g_n^{-1}[\tau + b_n^{-2}]\mathrm{cosec}^2 b_n$$
$$+\mu b_n^{-2}g_n^{-2}[2 - 3\mathrm{cosec}^2 b_n - 8\mu\mathrm{cosec}^2 b_n + 6\mu\mathrm{cosec}^4 b_n]\mathrm{cosec}^2 b_n\Big\}g_n^{-3}\mathrm{e}^{-b_n^2\tau}$$
$$+O(\ell^2). \qquad \text{(B 6}c\text{)}$$

REFERENCES

ABRAMOWITZ, M. & STEGUN, I. A. 1972 *Handbook of Mathematical Functions*. Dover.

ARIS, R. 1956 On the dispersion of a solute in a fluid flowing through a tube. *Proc. R. Soc. Lond.* A **235**, 67–77.

ARIS, R. 1959 On the dispersion of a solute by diffusion, convection and exchange between phases. *Proc. R. Soc. Lond.* A **252**, 538–550.

DAVIDSON, M. R. & SCHROTER, R. C. 1983 A theoretical model of absorption of gases by the bronchial wall. *J. Fluid Mech.* **129**, 313–335.

GILL, W. N. & SANKARASUBRAMANIAN, R. 1970 Exact analysis of unsteady convective diffusion. *Proc. R. Soc. Lond.* A **316**, 341–350.

JAYARAMAN, G., PEDLEY, T.J. & GOYAL, A. 1995 Dispersion of a solute in a fluid flowing through a curved tube with absorbing walls. In preparation.

LUNGU, E. M. & MOFFATT, H. K. 1982 The effect of wall conductance on heat diffusion in duct flow. *J. Engng Maths* **16**, 121–136.

PHILLIPS, C. G., KAYE, S. R. & SCHROTER, R. C. 1994 A diameter-based reconstruction of the branching pattern of the human bronchial tree. Part I. Description and application. *Respir. Physiol.* **98**, 193–217.

PURNAMA, A. 1988 Boundary retention effects upon contaminant dispersion in parallel flows. *J. Fluid Mech.* **195**, 393–412.

SANKARASUBRAMANIAN, R. & GILL, W. N. 1973 Unsteady convective diffusion with interphase mass transfer. *Proc. R. Soc. Lond.* A **333**, 115–132.

SHANKAR, A. & LENHOFF, A. M. 1991 Dispersion and partitioning in short coated tubes. *Ind. Engng Chem. Res.* **30**, 828–835.

SMITH, R. 1983 Effect of boundary absorption upon longitudinal dispersion in shear flows. *J. Fluid Mech.* **134**, 161–177.

TAYLOR, G. I. 1953 Dispersion of soluble matter in solvent flowing slowly through a tube. *Proc. R. Soc. Lond.* A **219**, 186–203.

TAYLOR, G. I. 1954 Conditions under which dispersion of a solute in a stream of solvent can be used to measure molecular diffusion. *Proc. R. Soc. Lond.* A **225**, 473–477.